CHAPTER ELEVEN

Energy System Alternatives

Part 2. MHD, Solar Energy, a Hydrogen Economy and Concluding Remarks

11.4 Magnetohydrodynamic Energy Conversion

Magnetohydrodynamic energy conversion, popularly known as MHD, is another form of direct energy conversion in which electricity is produced from fossil fuels without first producing mechanical energy. The process involves the use of a powerful magnetic field to create an electric field normal to the flow of an electrically conducting fluid through a channel, as suggested by Equation (11.13) and depicted in Figure (11.19). The flow velocity u is parallel to the channel axis, taken in the y-direction. The drift of electrons induced by this lateral electric field produces an electric current, represented by the current density vector **J**. Electrodes in opposite side walls of the MHD flow channel provide an interface to an external circuit. Electrons pass from the fluid at one wall to an electrode, to an external load, to the electrode on the opposite wall, and then back to the fluid, completing a circuit. Thus the MHD channel flow is a direct current source that can be applied directly to an external load or can be linked with a power-conditioning inverter to produce alternating current.

MHD effects can be produced with electrons in metallic liquids such as mercury and sodium or in hot gases containing ions and free electrons. In both cases, the electrons are highly mobile and move readily among the atoms and ions while *local net charge neutrality is maintained*. That is, while electrons may move with ease, any small volume of the fluid contains the same total positive charges on the ions and negative electron charges, because any charge imbalance would produce large electrostatic forces to restore the balance.

Though liquid metal MHD has been demonstrated experimentally, most theoretical and experimental work and power plant development and application studies have focussed on high-temperature ionized gas as the working fluid. Unfortunately, most common gases do not ionize significantly at temperatures attainable with fossil fuel chemical reactions. This makes it necessary to *seed* the hot gas with small amounts of vapor of readily ionizable materials such as the alkali metals. The resulting ions and electrons make the hot gas sufficiently electrically conducting that it may be influenced by the applied magnetic field.

The ionization potentials are measures of the energy needed to free valence electrons from an atom. Materials such as cesium and potassium have ionization potentials low enough that they ionize at the temperatures attainable with combustion

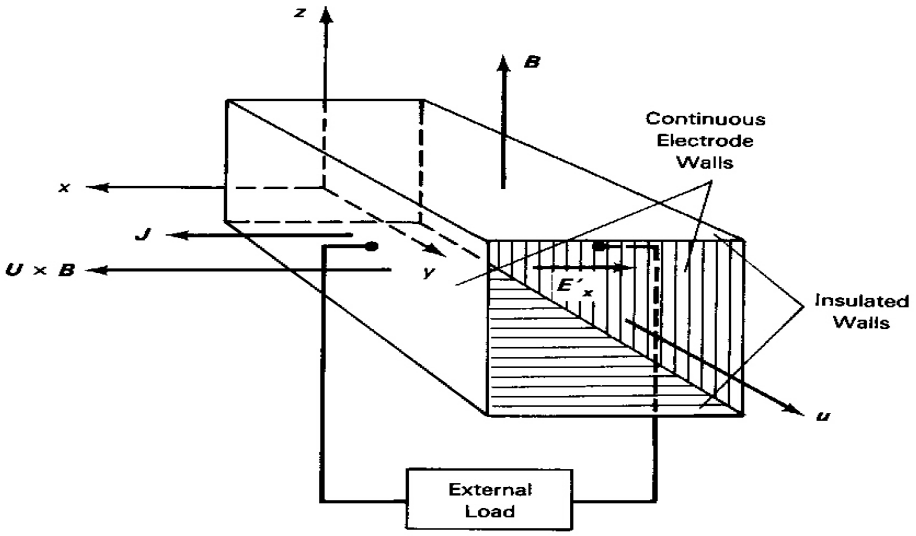

FIGURE 11.19 Magnetohyrodynamic (MHD) channel notation. Fluid motion in the *y*-direction through the magnetic field in the *z*-direction produces current flow in the *x*-direction (electron motion in the negative *x*-direction).

reactions in air. Recovery and reuse of seed materials from the MHD channel exhaust are usually considered necessary from both economic and pollution standpoints.

Ionized Gases in Electromagnetic Fields

Before analyzing the MHD channel, we will consider briefly the behavior of electrons in an ionized gas in the presence of electromagnetic fields.

In a gas at or near equilibrium, atoms, ions, and electrons are in random motion. At any given spatial position their velocities are distributed about a mean velocity that increases with increase in the local temperature. Consider just one of the free electrons moving, without collision, in a plane normal to a uniform magnetic field, as in Figure 11.20. The electron experiences a constant force qc_eB normal to its path according to Equation (11.11). Here, q is the charge of the electron and c_e the magnitude of its velocity. Because the force is normal to its path, the electron travels with constant velocity on a circular path around magnetic lines of force. By Newton's Second Law, the force on the electron is

$$F = m_e c_e^2/r = qc_eB \qquad [\text{N}] \qquad (11.21)$$

It follows that the angular frequency of the electron about a line of force c_e/r, called its *cyclotron frequency,* is

$$\omega = c_e/r = qB/m_e \qquad [\text{s}^{-1}] \qquad (11.22)$$

The electron cyclotron frequency is independent of electron velocity and is dependent

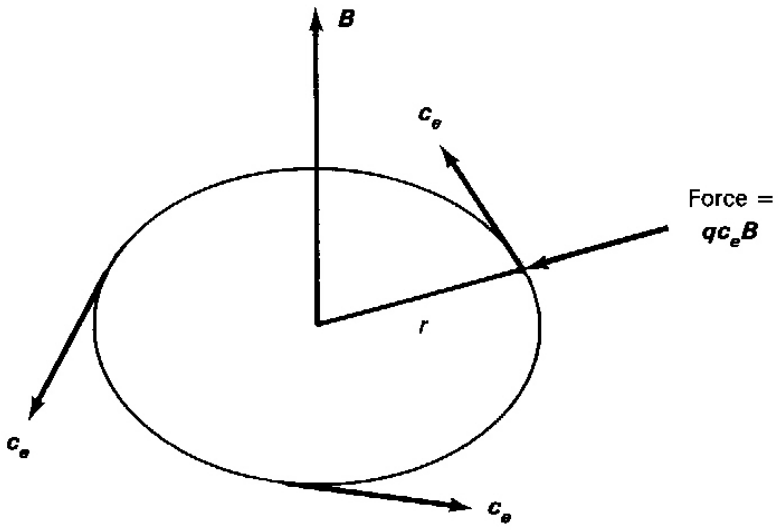

FIGURE 11.20 Circular orbit of an electron in a uniform magnetic field showing electron velocity vectors at several instances. The Lorentz force is always directed toward the center of the path.

only on the magnetic field strength and electron properties. Although the cyclotron motions of electrons exist in gases when strong magnetic fields are present, the circular paths of the electrons may be disrupted by collisions with other particles.

The likelihood of collisions between particles depends on their effective sizes: larger particles will collide more frequently. The probability of collision is taken as proportional to the collision cross-section Q of the particle, which may be thought of as its area. The frequency of collision of electrons ω_c is given by the product of the electron number density, n_e [electrons/m^3], the collision cross-section, Q [m^2], and the velocity, c_e [m/s]:

$$\omega_c = n_e Q c_e = 1/\tau \qquad \text{[collisions per s]} \qquad (11.23)$$

Here, the *mean time between collisions*, τ [s], is the inverse of the collision frequency.

The ratio of the cyclotron frequency to the collision frequency ω/ω_c, is called the *Hall parameter*. It indicates the relative importance of the magnetic field and collisions in controlling electron motion in the ionized gas. The Hall parameter is related to the magnetic field intensity by

$$\omega/\omega_c = \omega\tau = qB\tau/m_e = qB/n_e m_e Q c_e \qquad \text{[dl]} \qquad (11.24)$$

It is proportional to the number of cyclotron loops made per collision. A Hall parameter large compared with one indicates magnetic-field-dominated motion of

electrons, while a small value implies that collisions quickly break up ordered motions produced by the magnetic field.

At least three velocities are of importance in a conducting gas in a MHD channel. First, the velocity of the gas stream is given by **u** (assumed constant for the present case for an appropriately designed channel). Secondly, the velocities of individual electrons $\mathbf{c}_e$, as just introduced, are distributed about an average value that increases with the local temperature. In the absence of electromagnetic fields, the average value of $\mathbf{c}_e$ over all electrons is the flow velocity **u**; i.e., on the average the electrons move with the gas flow. When fields are present, however, there may be an average motion of electrons relative to the gas. It is the ease of this motion that determines the conductivity of the gas. The third velocity, the relative velocity of an electron $\mathbf{w}_e$, is defined as the vector difference of its absolute velocity and the mean fluid velocity:

$$\mathbf{w}_e = \mathbf{c}_e - \mathbf{u} \qquad [\text{m/s}]$$

The *drift velocity* w_e, is the magnitude of the average of the relative velocities of the electrons. In the absence of fields, the average of $\mathbf{c}_e$ is **u**, and thus the drift velocity is zero. When an electric field is present, however, the transport of negative charge by electrons represents a current flow in the gas.

Another important parameter, the *electron mobility* μ, is a measure of the response of electrons to an electric field. It is defined as the ratio of the magnitude of the electron drift velocity w_e to the local electric field intensity:

$$\mu = w_e/E \qquad [\text{m}^2/\text{V-s}] \qquad (11.25)$$

If it is assumed that an electron loses all of its drift velocity on collision, the acceleration of the electron may be approximated by the ratio of the drift velocity to the mean time between collisions. Because the force due to the electric field is given by qE, Newton's Second Law allows the drift velocity to be expressed as

$$w_e = qE\tau/m_e \qquad [\text{m /s}] \qquad (11.26)$$

The electron mobility can then be written as

$$\mu = q\tau/m_e \qquad [\text{m}^2/\text{V-s}] \qquad (11.27)$$

Using equation (11.24), the product μB becomes the Hall parameter:

$$\mu B = \text{q}\tau\text{B}/m_e = \omega\tau = \omega/\omega_c \qquad [\text{dl}] \qquad (11.28)$$

Thus the Hall parameter is large for gases of high electron mobility in strong magnetic fields. It will be seen that this can have a significant effect on MHD channel design.

Assuming electrons as the dominant charge carriers, the current density can also

be related to the electron mobility through the drift velocity:

$$J = n_e q w_e = n_e q^2 \tau E / m_e$$

$$= \mu n_e q E \qquad [\text{A/m}^2] \qquad (11.29)$$

The electron conductivity of a stationary gas is then given by:

$$\sigma = J/E = \mu n_e q \qquad [(\Omega\text{-m})^{-1}] \qquad (11.30)$$

Thus high electron mobility and electron number density are essential to achieve the high conductivity needed in an MHD generator.

Analysis of a Segmented Electrode MHD Generator

Consider the one dimensional flow of a gas in an MHD channel coupled with a simple three-dimensional model of the electromagnetic phenomena. Rather than the continuous electrode configuration shown in Figure 11.19, we examine a refined configuration, shown in Figure 11.21. Here the electrodes, set in opposite electrically insulated channel walls, are segmented in the streamwise direction. This eliminates a return path along the wall for axial electrical currents in the flow.

By the same notation as in Figure 11.19, a seeded, ionized gas flows through the segmented-electrode channel in the *y*-direction with a constant velocity *u*. A uniform magnetic field in the *z*-direction exists throughout the gas in the channel. A force given by $q\mathbf{u}\times\mathbf{B}$, and thus an equivalent electric field $\mathbf{u}\times\mathbf{B}$ is imposed on the flow in the channel. Therefore, positive ions tend to drift in the positive *x*-direction and electrons drift in the negative *x*-direction toward the right electrodes. Because their mobility is much greater than that of the relatively massive ions, the electrons are the primary charge carriers. The electrons are collected at the right electrodes and flow through the external circuits returning to the channel at the left electrodes, as shown in Figure 11.21.

When the channel is under an electrical load, the current density vector in the *x*-direction induces a force on the fluid in the negative *y*-direction. Thus the *x*-component of *J* interacts with the magnetic field to produce the axial electric field component $E_y = -JB$ that opposes the flow velocity *u*. In order to maintain a constant velocity in the duct, a streamwise pressure gradient, *dp/dy,* must balance the force due to this axial electric field and the viscous forces. Thus, ignoring viscous resistance, the axial force on the gas per unit volume is

$$F_y = -|\mathbf{J}\times\mathbf{B}| = -JB = dp/dy \qquad [\text{N/m}^3] \qquad (11.31)$$

where the negative sign indicates that the magnetic force is directed upstream. As a

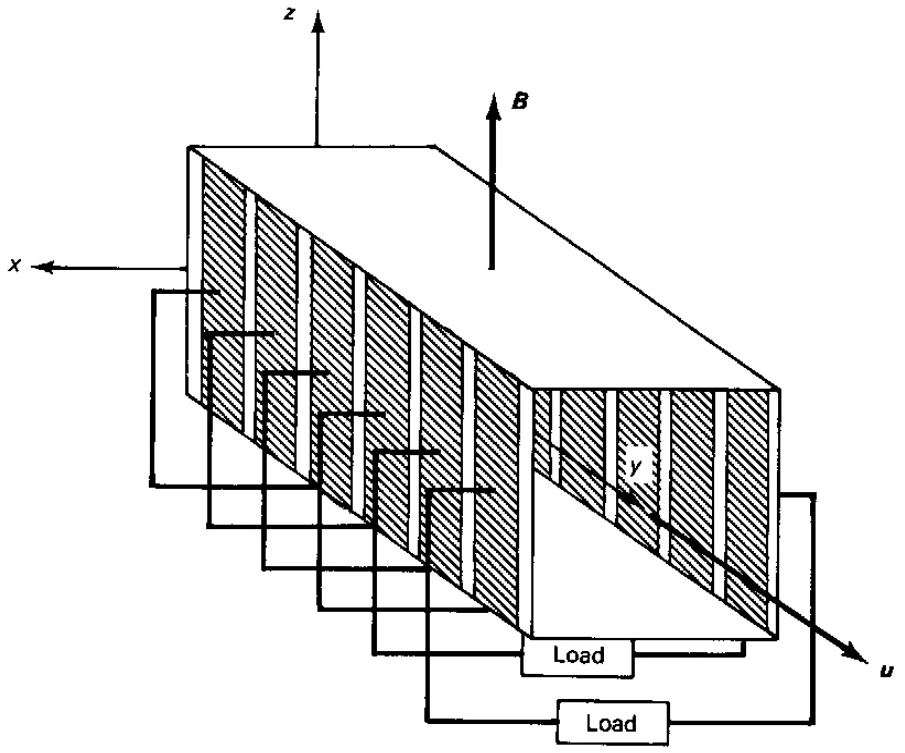

FIGURE 11.21 Segmented electrode MHD generator with individual loads.

result $dp/dy < 0$, indicating that the flow pressure drops as y increases. The resulting net pressure force in the positive y-direction balances the magnetic and viscous forces and maintains the flow velocity constant. A compressor is therefore required upstream of the channel to pressurize the flow, to support the field-induced streamwise pressure gradient, and thus to maintain the steady flow in the channel.

With segmented electrodes there is no axial current in the channel ($Jy = 0$), and thus the current density component $J_x = J$ is proportional to the net electric field in the x- direction:

$$J = \sigma(uB - E_x) \qquad [\text{A/m}^2] \qquad (11.32)$$

The combined electrical resistance of the MHD channel flow and the external load governs the available potential at the MHD electrodes. If the external circuit is open, $J = 0$; hence, Equation (11.32) indicates that $E_x|_{open} = uB$. With a finite external resistance, current flows and the electrode potential is reduced below the open-circuit value. Thus, under load, the channel voltage drops to a fraction K of the open-circuit voltage. Hence, we may write $E_x = KuB$, where K is called the *channel load factor* and where $0 \le K \le 1$. The current density then becomes

$$J = \sigma u B(1 - K) \qquad [\text{A/m}^2] \qquad (11.33)$$

The electrical power delivered to the load per unit volume of channel is then given by

$$\text{Power}|_{\text{out}} = \mathbf{J}\cdot\mathbf{E} = \sigma u^2 B^2 K(1 - K) \qquad [\text{W/m}^3] \qquad (11.34)$$

Returning now to consideration of the streamwise electrical fluid interaction, we write the steady-flow form of the First Law for an adiabatic control volume, including the work done against the body force, as

$$m(h_1 + u_1^2/2) = m(h_2 + u_2^2/2) + mw \qquad [\text{J/s}] \qquad (11.35)$$

where m is the channel mass flow rate. Work is positive here because it is done by the fluid in the channel to produce the electrical current flow to the external load. For constant velocity in the channel, this becomes

$$h_2 = h_1 - w = h_1 - (\text{Power}|_{\text{out}})(\text{Volume})/m$$

$$= h_1 - \sigma u^2 B^2 K(1 - K)/\rho \qquad [\text{kJ/kg}] \qquad (11.36)$$

where ρ is the gas density. Thus the work delivered to the load reduces the thermal energy of the flow. We have seen that a compressor is required to pressurize the flow in the channel and that heating of the flow provides a high entrance enthalpy and work output.

From Equations (11.31) and (11.33), the electrical retarding force on the flow is

$$F_y = -\sigma u B^2 (1 - K) \qquad [\text{N/m}^3] \qquad (11.37)$$

and the fluid power to push the gas through the channel per unit volume is

$$\text{Power}|_{\text{in}} = |F_y u| = \sigma u^2 B^2 (1 - K) \qquad [\text{W/m}^3] \qquad (11.38)$$

The Ohmic or I^2R loss is given, using Equation (11.33), by

$$J^2/\sigma = [\sigma u B(1 - K)]^2/\sigma = \sigma (uB)^2(1 - 2K + K^2)$$

$$= \sigma u^2 B^2(1 - K) - \sigma u^2 B^2 K(1 - K) \qquad [\text{W/m}^3] \qquad (11.39)$$

Comparing equations (11.34) and (11.38) with equation (11.39), we see that the ohmic loss is the difference between the power required to push the flow through the channel and the useful power through the load.

The efficiency of the channel is defined as the ratio of the $\text{Power}|_{\text{out}}$ to $\text{Power}|_{\text{in}}$. By Equations (11.34) and (11.38), the MHD channel efficiency is

$$\eta = \text{Power}|_{out} / \text{Power}|_{in} = K \qquad [\text{dl}] \qquad (11.40)$$

Thus the electrical efficiency of the segmented electrode MHD channel is equal to the channel load factor. Examination of Equation (11.34) shows that the power output vanishes when $K = 0$ and when $K = 1$. Thus there must be an intermediate value of K that maximizes the power output. By differentiation of Equation (11.34) with respect to K, the usual methods of calculus indicate that the power is maximized when $K = 0.5$. Thus operation at this value implies that 50% of the flow energy input to the channel is converted to electricity, and the remainder is dissipated in the flow channel. This energy is not lost from the flow but is an irreversibility that is reflected in a loss in ability of the flow to do work.

EXAMPLE 11.6

A 10-m^3 MHD generator with segmented electrodes has a short-circuit current density of 12,000 amperes per square meter. The gas conductivity is 20 $(\text{Ohm-m})^{-1}$.

If flow and magnetic field conditions are unchanged when the load factor is 0.6, what is the output power? What is the actual current density in the channel? If the magnetic field is doubled in strength, by what factor would you expect the output power to change?

Solution

For a short-circuit condition, the load factor is zero, and Equation (11.33) yields

$$J_{sc} = \sigma u B = 12000 \text{ A/m}^2$$

Then

$$uB = J_{sc}/\sigma = 12000/20 = 600 \text{ V/m}.$$

The power output is then given by Equation (11.34):

$$\text{Power} = \sigma u^2 B^2 K(1 - K)V = 20(600)^2(0.6)(0.4)(10) = 17{,}280{,}000 \text{ W} = 17.28 \text{ MW}$$

The channel current density is then given by

$$J = \sigma u B(1 - K) = 20(600)(0.4) = 4800 \text{ A/m}^2.$$

If the magnetic field strength is doubled, Equation (11.34) shows that the power output is increased by a factor of four, assuming there is no change in the flow or load conditions.

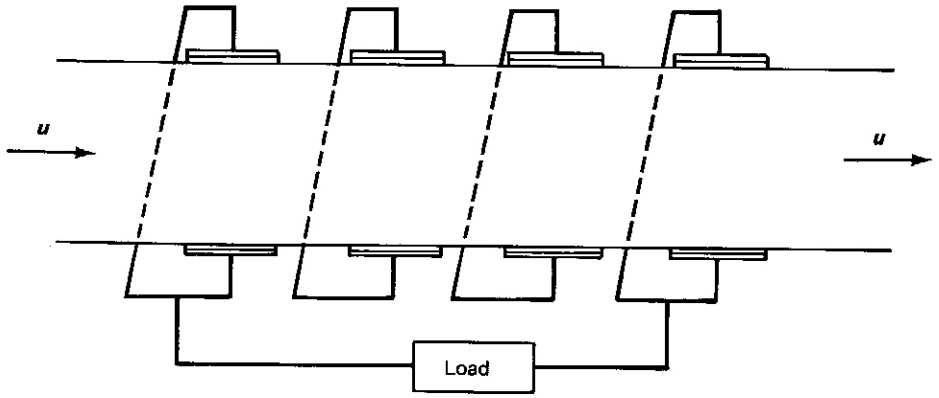

FIGURE 11.22 Electrode configuration for a Hall MHD generator.

Other MHD Configurations

The preceding discussion of the segmented electrode MHD channel provides a brief insight into the fundamentals of MHD power. Other electrode configurations include the Faraday continuous electrode generator and the so-called Hall generator. In the former case, with continuous electrodes, the electric field in the y-direction leads to a streamwise electrical current in a circuit that is completed in the continuous conducting electrodes. The resulting current along the channel axis, called the *Hall current*, contributes nothing to external power delivered in the Faraday generator. It is shown in references 1 and 44 that the power output for the continuous electrode generator is influenced by the Hall parameter and is given by Equation (11.34) with the right-hand side divided by the factor $1 + (\mu B)^2$. Thus high values of the Hall parameter drastically reduce the channel power output relative to the segmented electrode generator.

Rather than attempting to circumvent the Hall current, the Hall generator seeks to employ it by using the electrode configuration shown in Figure 11.22. In the Hall configuration, the electrodes are designed to short circuit the cross-channel electric current and pass the axial Hall current through the load. The Hall generator power output also depends on the Hall parameter, but in a more complex way than in the continuous electrode Faraday configuration. The reader is referred to references 1 and 44 for further detail.

MHD channels, like gas turbines, may be operated on open or closed cycles. Normally, combustion-driven MHD systems use an open-cycle, such as that shown in Figure 11.23, where pressurized combustion takes place upstream of the MHD channel. As with the gas turbine, the temperature of the channel exhaust is high, making it advantageous to employ regenerative heat exchange and/or a bottoming cycle such as the steam turbine in Figure 11.23. For MHD channels with steam bottoming cycles, overall efficiencies in the range of 50–60% are predicted.

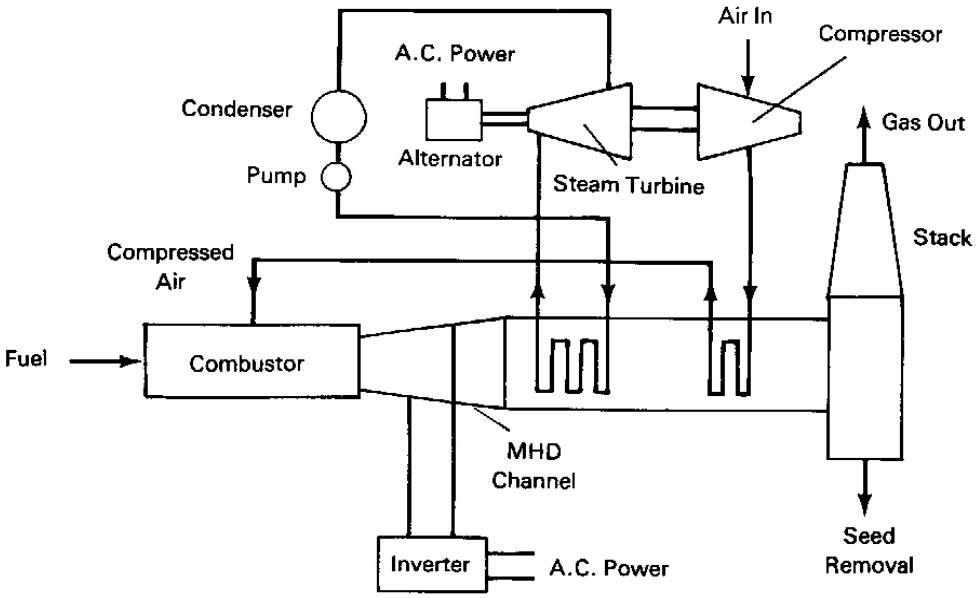

FIGURE 11.23 MHD generator with steam bottoming cycle. Compressed air or oxygen preheated in the exhaust duct downstream of the MHD channel mixes with fuel and seed material in the combustor to form an ionized flow through the channel. MHD DC is converted to AC with an inverter. The channel exhaust is cooled by producing steam for the bottoming Rankine cycle.

If a DC source, rather that a load, is applied to the electrodes of a properly contoured Faraday channel, the energy in the flow may be increased and the flow accelerated. The electric field in this case exceeds the uB term in Equation (11.32), reversing the direction of the current density and thus the direction of the $\mathbf{J} \times \mathbf{B}$ force. The MHD channel may then be used for propulsion through expulsion of mass in the same way as in a jet engine or rocket.

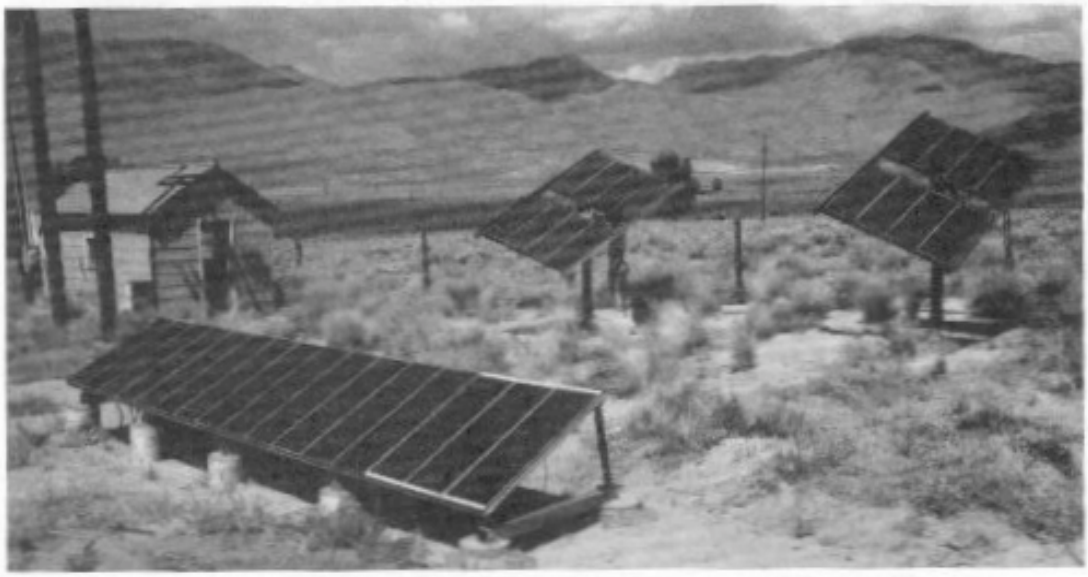

FIGURE 11.24 Two types of solar photovoltaic collectors at a remote site in Bishop, Calif. (Courtesy of Southern California Edison.)

11.5 Solar Energy

The preceding pages have dealt with the conversion of energy from fossil and nuclear fuels, all finite resources. While the need may not be immediate, the day is approaching when the Earth's fossil and nuclear resources will no longer satisfy man's need to grow and prosper. We must therefore consider more seriously the effective utilization of the readily available and, for practical purposes, eternal energy source provided by the sun.

Ancient peoples learned to use the sun for survival and comfort. Not very long ago a clothesline and wind formed the mechanism of a solar clothes dryer. Powered by the sun, the atmospheric engine that produces weather change provides the wind to fill sails and turn windmills to produce small amounts of power at a few select locations. Passive solar architecture has recently attracted widespread interest, and solar collectors mounted on roofs for water heating and space heating have become commonplace in many areas. Figure 11.24 shows fixed and tracking solar arrays that produce electricity to supplement or replace grid power at a remote location.

A major problem connected with using the sun for power generation is the same characteristic that allows the survival of human life on earth: the low intensity levels of solar radiation. It is well known that the two planets closest to the sun have average temperatures higher than the Earth's and that the outer planets are colder because of the inverse square law of radiative transfer of the sun's radiation field. Higher solar fluxes at Earth's surface would clearly make the sun a more easily engineered radiation source. Let us estimate the intensity of the solar radiation arriving at Earth.

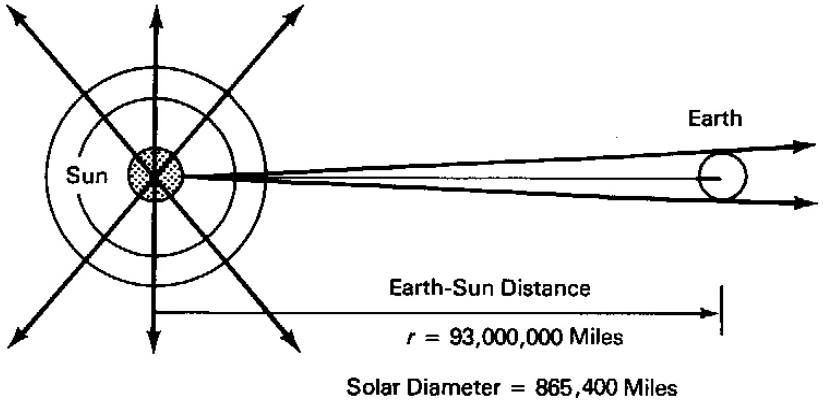

FIGURE 11.25 Earth–sun geometry and the spherically symmetric radiation field of the sun.

Consider the geometry of the Earth–sun system and the spherically symmetric nature of the sun's radiation field presented in Figure 11.25. Assuming that the sun radiates energy uniformly in all directions at a rate of E kW, the radiant flux density Φ crossing any sphere concentric with the sun is given by dividing E by the area of the sphere. Thus the *radiant flux density*, or *irradiance*, at a distance r from the sun center is

$$\Phi = E/(4\pi r^2) \qquad [\text{kW/m}^2] \qquad (11.41)$$

In order to evaluate Φ, it is necessary to calculate the rate of energy emitted by the sun per unit area of its surface, Φ_s. While the temperature at the center of the sun is much hotter, solar radiation approximates *blackbody radiation* at a temperature of 5762 K. Using the Stefan-Boltzmann constant, $\sigma = 5.66961 \times 10^{-8}$ W/m^2-°K^4, the *blackbody radiation law* (discussed later in more detail) gives the rate of energy emission per unit area of the sun's surface as

$$\Phi_s = \sigma T^4 = 5.66961 \times 10^{-8} (5762)^4 (10^{-3}) = 62{,}495 \text{ kW/m}^2$$

Applying conservation of solar energy to concentric spheres makes it clear that energy emitted uniformly from a sphere at the sun's radius r_s will be distributed over a wider area when passing through a sphere of larger radius. Thus, eliminating E for two concentric spheres from Equation (11.41) shows that radiant flux density scales inversely as the area ratio or square of the radius ratio of the spheres:

$$\Phi = \Phi_s (r_s/r)^2 \qquad [\text{kW/m}^2] \qquad (11.42)$$

This and Equation (11.41) are both mathematical expressions of the inverse square law for solar radiation.

As in Figure 11.25, taking the sun's diameter to be 865,400 miles and the Earth–sun distance as 93,000,000 miles, the solar radiant flux density, or *solar constant* of radiation, reaching Earth's orbit is

$$\Phi_e = \Phi_s(r_s/r_e)^2 = 62{,}495[(865{,}400/2)/93{,}000{,}000]^2 = 1.353 \text{ kW/m}^2$$

Thus the value of the solar constant is the rate at which solar radiation crosses a unit area normal to the sun's rays at the distance of Earth from the sun. A more precise value for the solar constant is $\Phi_e = 1.357$ kW/m^2, or 430.2 Btu/hr-ft^2 (ref. 39).

While solar radiation may be viewed as a divergent spherical radiation field on the scale of the solar system, a calculation of the angle of divergence at the earth's distance indicates that its rays are essentially parallel on the scale of almost all human activities. Thus it is common to assume a constant radiation flux density with parallel rays in analyzing terrestrial solar radiation problems.

Some of the solar radiation arriving at the earth's surface is scattered and reflected in the atmosphere. Thus solar radiation consists of direct (parallel) and diffuse components. Moreover, absorption, reflection, and scattering in the atmosphere reduces the maximum direct radiation flux density arriving at sea level to about $\Phi_{dir} = 1$ kW/m^2. When the sky is clear, the direct component dominates. But the direct component may essentially vanish on overcast days, leaving only a diffuse component. The calculation of the solar performance of space vehicles is usually simplified by the absence of a diffuse component. However, for near-Earth satellites, radiation emitted from Earth and solar radiation reflected from Earth could be significant.

Matter interacts with solar radiation in three basic ways: it can absorb the radiation, transmit it, or reflect it. These actions are represented by characteristics called, respectively, *absorptance A*, *transmittance T*, and *reflectance R*. Each is expressed as a fraction of the total incident radiation. Thus the radiation energy reflected from a surface with reflectance R and a given area S is $RS\Phi$.

Consider a layer of material with surface area S normal to a radiation field with radiant flux Φ. Conservation of energy requires that the rate of energy incident on the surface equal the sum of the rates of energy reflected, transmitted, and absorbed. Thus $\Phi S = RS\Phi + TS\Phi + AS\Phi$. Thus the sum of the reflectance, the transmittance, and the absorptance must equal 1:

$$R + T + A = 1 \qquad \text{[dl]} \qquad (11.43)$$

Let us apply this statement of energy conservation to the Earth's atmosphere: On a clear day, the atmospheric reflectance is small, hence any radiation not absorbed is transmitted to the surface ($T + A \approx 1$). On a cloudy day, reflection from and absorption by clouds are significant, and the transmitted radiation becomes a small fraction of the incoming solar irradiance ($R + A \approx 1$); only the diffuse component scattered by the clouds remains.

Spectral Characteristics

Though it is usually convenient to deal with total radiation quantities, sometimes it is necessary to consider wavelength-dependent, or spectral, effects. The material radiative properties just introduced above are sometimes frequency or wavelength dependent. Thus, while solar radiation in space approximates a blackbody spectral distribution, radiation penetrating to Earth's surface deviates significantly from the blackbody distribution because of scattering and strong absorption bands due to atmospheric water vapor, carbon dioxide, dust, and other substances that remove significant amounts of energy from the incident radiation at certain wave lengths.

The eye itself is a highly wavelength-selective radiation sensor, being limited to observing radiation only in the range of about 0.4 to 0.7 microns. A micron is 10^{-6} meters.

Consider the *Planck equation for the blackbody spectral distribution of radiation* $F_b(\lambda)$, where wavelength λ is in microns [μ] (refs. 37, 43 and 55):

$$F_b(\lambda) = 2\pi hc^2\lambda^{-5}/(e^{hc/(k\lambda T)} - 1) \qquad [\text{Btu}/(\text{ft}^2\text{-hr-}\mu) \mid \text{W}/(\text{m}^2\text{-}\mu)]$$

The Planck equation may be written in terms of a single parameter λT, where wavelength is in microns and temperature is in appropriate absolute units:

$$F_b(\lambda T)/T^5 = 2\pi hc^2 (\lambda T)^{-5}/(e^{hc/(k\lambda T)} - 1)$$

$$= 3.742\times10^8(\lambda T)^{-5}/(e^{14381/(\lambda T)} - 1) \qquad [\text{W}/(\text{m}^2\text{-}\mu\text{-}^\circ\text{K}^5)] \qquad (11.44a)$$

$$= 1.187\text{x}10^8(\lambda T)^{-5}/(e^{25896/(\lambda T)} - 1) \qquad [\text{Btu}/(\text{ft}^2\text{-hr-}\mu\text{-}^\circ\text{R}^5)] \qquad (11.44b)$$

Figure 11.26 shows the Planck blackbody radiation distributions for two different temperatures as a function of wave length, one approximating solar radiation at 10,000 °R (5555.5°K) and the other much closer to, but above, the normal terrestrial temperature of 1000°R (555.5°K). At first glance the radiation levels appear comparable; but they actually they are vastly different from each other (by a factor of 10^5), because the Planck function is divided by σT^5, to allow display on the same scale.

The figure makes clear that in the spectral range to which the eye is sensitive, the visible range, little radiation emitted by relatively cool terrestrial objects is visible; and almost all of what we see is reflected solar radiation or other high-temperature-source radiation (such as from high-temperature lamp filaments or from flames). The vast difference in the wave lengths of the peaks shows why it is important to consider spectral effects in dealing with solar radiation.

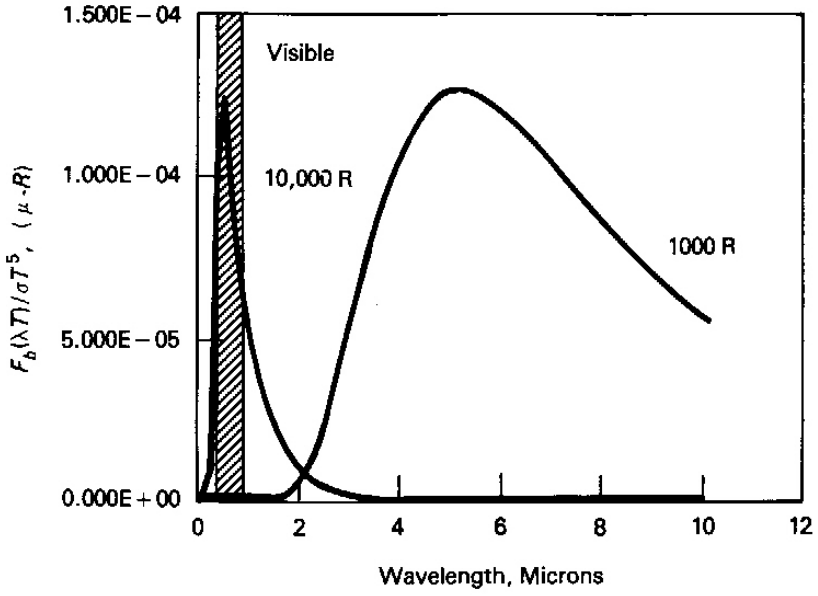

FIGURE 11.26 Spectral distributions of blackbody radiation. Note that the Planck functions are divided by the fifth power of the absolute temperature so that both may be displayed on the same scale.

The Wien displacement law, a simple relation derivable from the Planck equation, given in both English and SI units,

$$\lambda_{max}T = 5215.6 \qquad [\mu\text{-°R}] \qquad (11.45a)$$

$$= 2897.6 \qquad [\mu\text{-°K}] \qquad (11.45b)$$

shows that the wavelength of the peak of the blackbody radiation distribution, λ_{max}, is inversely proportional to the temperature, as may be verified numerically for the two peaks in Figure 11.26 ($\lambda_{max} = 5.215\mu$ and 0.5215μ).

Integration of F_b over all wavelengths from zero to infinity, using Equation (11.44) yields the Stefan-Boltzmann law for the blackbody flux Φ_b:

$$\Phi_b = \int_0^\infty F_b\, d\lambda = T^4 \int_0^\infty [F_b(\lambda T)/T^5]\,d(\lambda T) = \sigma T^4 \qquad [\text{Btu/hr-ft}^2|\text{W/m}^2] \qquad (11.46)$$

which was used earlier to estimate the radiative flux from the surface of the sun and the terrestrial solar constant.

It is useful to sum the contributions to blackbody emission from zero to a given wavelength by an integration of F_b, as was done for the entire spectral range in Equation (11.46). Letting $\alpha = \lambda T$, we define a function $\Sigma(\lambda T)$ as a dimensionless fraction of the blackbody irradiance from $\alpha = 0$ to $\alpha = \lambda T$:

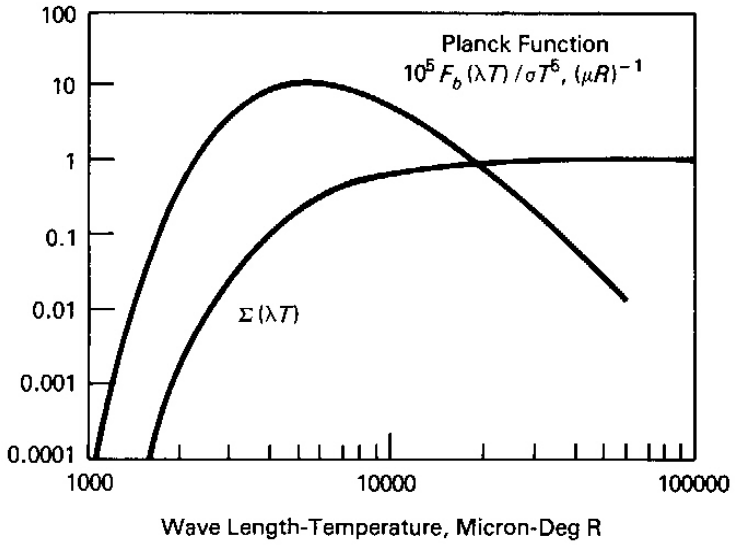

FIGURE 11.27 Universal blackbody distribution functions. Note that the Planck function and Σ function here depend only on the wavelength–temperature product.

$$\Sigma(\lambda T) = T^4/\Phi_b \int_0^{\lambda T} [F_b(\alpha)/T^5]d\alpha \qquad [dl]$$

Figure 11.27 shows a log-log graph of the Planck distribution and $\Sigma(\lambda T)$. A table of the latter function, calculated by numerical integration using a spreadsheet, is provided in Appendix I. The dimensional blackbody flux between any two wave lengths for a given temperature may be determined from a difference of sigma functions as:

$$\Phi(\lambda T)_2 - \Phi(\lambda T)_1 =$$

$$= T^4 \int_{(\lambda T)1}^{(\lambda T)2} [F_b(\alpha)/T^5]d\alpha = [\Sigma(\lambda T)_2 - \Sigma(\lambda T)_1]\sigma T^4 \qquad [Btu/hr\text{-}ft^2|W/m^2]$$

EXAMPLE 11.7

Consider a window, normal to the sun's rays, covering a solar collector mounted on a satellite in near-Earth orbit. The window has a transmittance of 0.9 in the range of wavelengths from 0.2–2.0 μ and 0 at other wavelengths. What is the fraction of incident solar radiation transmitted by the window, and what is the rate of useful energy transfer to a circulating fluid in a 4 × 4-m flat plate collector if the collector absorbs 85% of the transmitted radiation?

Solution

The only radiation transmitted is between 0.2 and 2.0 μ. Because the effective temperature of the solar radiation is 10,000° R, the values of λT and Σ for these two wavelengths are

$\lambda T = (0.2)(10000) = 2000\ \mu\text{-°R}$ and $\Sigma(2000) = 0.0013$

and

$\lambda T = (2.0)(10000) = 20{,}000\ \mu\text{-°R}$ and $\Sigma(20{,}000) = 0.934$

using the Σ table in Appendix I.

The transmitted fraction of the blackbody incident radiant energy is the product of the fraction of radiation in the transmitted spectral range and the window transmittance:

$$(0.9)(0.934 - 0.0013) = 0.839$$

The radiation that heats the circulating fluid is then the product of the transmitted spectral fraction, the absorptance, the area, and the near-earth solar constant:

$$(0.839)(0.85)(4^2)(1.357) = 15.5 \text{ kW}.$$

Example 11.7 dealt with a constant transmittance over a single spectral interval. More complex radiation characteristics may be treated in a similar way by summing the contributions of more than one spectral band.

Earth-Sun Geometry and Solar Collectors

Radiative transfer from the sun to a plane surface depends on the orientation of the surface to the sun's rays. If parallel rays irradiate a surface, the total energy rate per unit area is given by the product of the irradiation Φ and the cosine of the angle between the surface normal and the sun's rays: $\Phi\cos\theta$. The following discusses ways in which the cosine function can be evaluated.

Consider the component of radiation falling on a terrestrial horizontal surface with unit normal **n**, when the sun's rays are in the direction of a second unit vector **s**. Following the notation of Figure 11.28, the two unit vectors **n** and **s** can be expressed in terms of the orthogonal unit vectors **i**, **j**, and **k**:

$$\mathbf{n} = n_x\mathbf{i} + n_y\mathbf{j} + n_z\mathbf{k} \quad \text{and} \quad \mathbf{s} = s_x\mathbf{i} + s_y\mathbf{j} + s_z\mathbf{k}$$

where n_x, n_y, n_z, and s_x, s_y and s_z are the direction cosines of the two vectors. Note that the direction cosines must satisfy the following conditions:

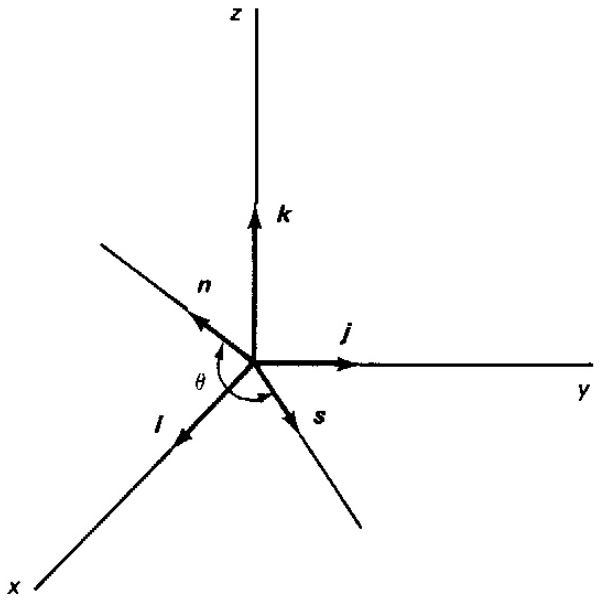

FIGURE 11.28 Unit vectors for solar position analysis. The origin of the coordinates is at Earth's center, **n** is normal to a horizontal surface on Earth, and **s** points at the sun. θ is the angle between the two vectors.

$$\mathbf{n} \cdot \mathbf{n} = n_x^2 + n_y^2 + n_z^2 = 1 \qquad \text{and} \qquad \mathbf{s} \cdot \mathbf{s} = s_x^2 + s_y^2 + s_z^2 = 1$$

for **n** and **s** each to be of unit magnitude. The fraction of the maximum solar radiation falling on the unit area, then, is given by the scalar product:

$$\cos\theta = \mathbf{n} \cdot \mathbf{s} = n_x s_x + n_y s_y + n_z s_z \tag{11.47a}$$

Figure 11.29 shows these unit vectors set at the center of the earth. The unit vector **n** points to the zenith of the observer and is normal to the horizontal surface at P. Here the *x*-axis is taken through the intersection of the meridional plane containing **n** and the equatorial plane. The *z*-axis points north and the *y* axis is selected to complete a right-handed coordinate system. The angle *L* is the latitude of **n**. In this system the position of the sun is determined by two convenient angles: *H* and δ. Examination of Figure 11.29 shows that the components of **s** on the coordinate axes are

$$s_x = \cos\delta\cos H \qquad s_y = \cos\delta\sin H \qquad \text{and} \qquad s_z = \sin\delta$$

Similarly, $n_x = \cos L$, $n_y = 0$, and $n_z = \sin L$. Thus the cosine of the sun-surface angle given by $\mathbf{n} \cdot \mathbf{s}$ using Equation (11.47a) is

$$\cos\theta = \cos\delta\cos H\cos L + \sin\delta\sin L \tag{11.47}$$

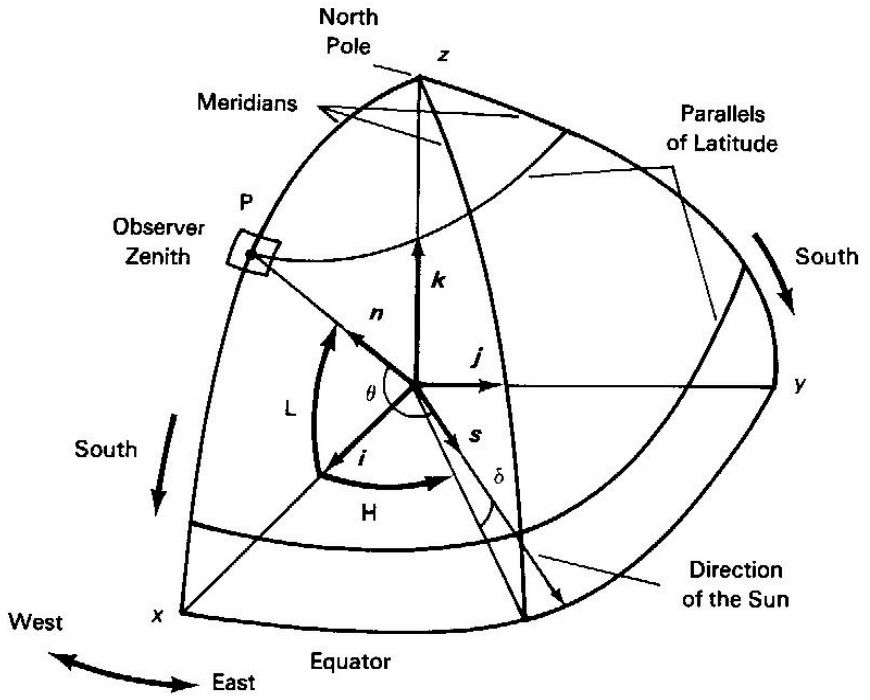

FIGURE 11.29 Earth-centered solar and observer angles. *L* is the latitude of the surface of interest, δ is the elevation of the sun, and *H* is the hour angle of the sun from the observer's longitude.

Thus the cosine of the angle of the sun's rays falling on a horizontal surface depends on the latitude of the surface and the angles H and δ of the sun.

Now consider the determination of *H* and δ. First we define the *ecliptic* as the plane of earth's annual motion around the sun, as shown in Figure 11.30. Because the earth's axis always points in approximately the same direction in space and is inclined at 23.5° to the normal to the ecliptic, the apparent position of the sun as viewed from Earth ranges above and below the equator by 23.5° annually. This movement is designated by the solar *declination angle* δ in Figure 11.29, measured from the equatorial plane along a meridian of longitude. It can be seen from Figure 11.30 that δ varies from + 23.5° degrees on June 21 to – 23.5° on December 21.

The *hour angle H* of the sun in Figure 11.29 is the angle measured in the plane of the equator between the observer's meridional plane and the meridional plane of the sun. Earth rotates once or 360° about its axis in 24 hours; hence, the hour angle depends on time, as its name implies. If *solar time* is measured from solar noon (when the sun is at its highest point in the sky at the observer's meridian), the hour angle may be computed from the solar time using the factor 360/24 = 15° per hour. The hour angle is positive when the sun is east of the observer and negative when it is west. Thus at 3:00 P.M. solar time, the sun is 3 hours past solar noon and, therefore, has an hour angle of 3×(–15) = – 45° (west of the observer).

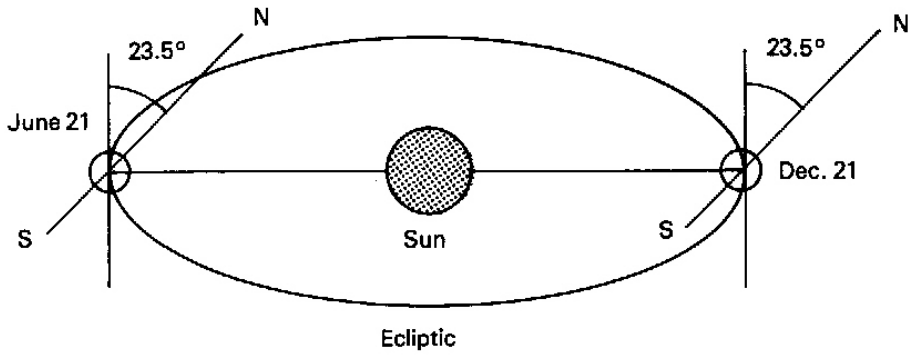

FIGURE 11.30 Inclination to the ecliptic of Earth's axis. The Earth's axis always points in the same direction as it revolves around the sun.

Care should be taken to distinguish between solar time and time defined by law called *civil time*. In the continental United States, for instance, there are four time zones defined by law in which *standard time* decreases by one hour for each 15° of longitude from the east to the west coast. This allows a uniform time within a zone while approximating solar time. Exceptions have been made to accomodate irregular state boundaries. Thus standard time deviates from solar time by several minutes, depending on the longitude of the observer. Moreover, by law, *daylight saving time* differs from standard time. In the spring and fall, clocks are advanced and set back an hour, respectively. Under daylight saving time, the civil time in the summer would be 1 pm at any location where it is noon standard time. Thus solar time can deviate from daylight saving time by more than an hour at some locations.

EXAMPLE 11.8

What is the incident radiative energy rate falling on a 7 × 10-m horizontal roof on a clear day at 40° north latitude, at a solar time of 10 A.M. on December 21?

Solution

Figure 11.30 shows that on December 21 the solar declination angle $\delta = -23.5°$. At 10 A.M. sun time, the hour angle is 2 hr × 15°/hr = 30°. By Equation (11.47), the angle of the sun relative to the roof vertical is

$$\cos\theta = \cos\delta\cos H\cos L + \sin\delta\sin L$$

$$= \cos(-23.5°)\cos(30°)\cos(40°) + \sin(-23.5°)\sin(40°) = 0.352.$$

Taking the solar constant at Earth's surface as 1.0 kW / m^2, the incident energy on the roof is

$$(0.352)(70)(1.0) = 24.64 \text{ kW}$$

Note that the solar angle θ is independent of the sign of the hour angle. Thus $\cos\theta$ is a symmetric function of H, and the same irradiance occurs at 10 A.M. and 2 P.M. solar time.

EXAMPLE 11.9

What is the irradiance on an east-facing vertical wall in kW / m^2, under the conditions of Example 11.8?

Solution

A unit vector on an east-facing wall at the observer location in Figure 11.29 is directed along the y-axis and is therefore simply **j**. The cosine of the angle between the east-facing-wall normal and the solar direction vector **s** is

$$\mathbf{j} \cdot \mathbf{s} = s_y = \cos\delta \sin H = \cos(-23.5°)\sin(30°) = 0.4585$$

The solar irradiance is then (1.0)(0.4585) = 0.4585 kW/m^2. Here, the hour angle dependency is antisymmetric. It would give a negative result for 2 P.M. solar time ($H = -30°$). Thus, after solar noon, when $\mathbf{j} \cdot \mathbf{s} < 0$, the negative sign indicates that the sun is behind the east-facing wall and that the wall of the building is in the shade.

Solar collectors can be fixed in position or they can track the sun. Fixed collectors for year-round use in the northern hemisphere are normally oriented facing the south with a tilt angle β that is approximately equal to the collector latitude. For a south-facing collector tilted at an angle β with respect to the horizontal, the collector normal makes an angle of $L - \beta$ with the equatorial plane in Figure 11.29. The angle of the collector normal, **n**, with the sun direction may then be determined using

$$\mathbf{n} = \underline{\mathbf{i}} \cos(L - \beta) + \mathbf{k} \sin(L - \beta)$$

Then $\cos\theta$ is

$$\cos\theta = \mathbf{n} \cdot \mathbf{s} = \cos(L - \beta)\cos\delta \cos H + \sin(L - \beta)\sin\delta$$

Note that this equation may also be obtained by replacing the latitude in Equation (11.47) with $L - \beta$.

For sun-tracking solar collectors, two degrees of angular freedom are required for perfect tracking. Typically, such collectors would pivot about horizontal and vertical axes dictated by the local solar azimuth and elevation. Their angular motion may be preprogrammed using astronomical data such as those from reference 56, or, it could be controlled by a sun-seeking control system.

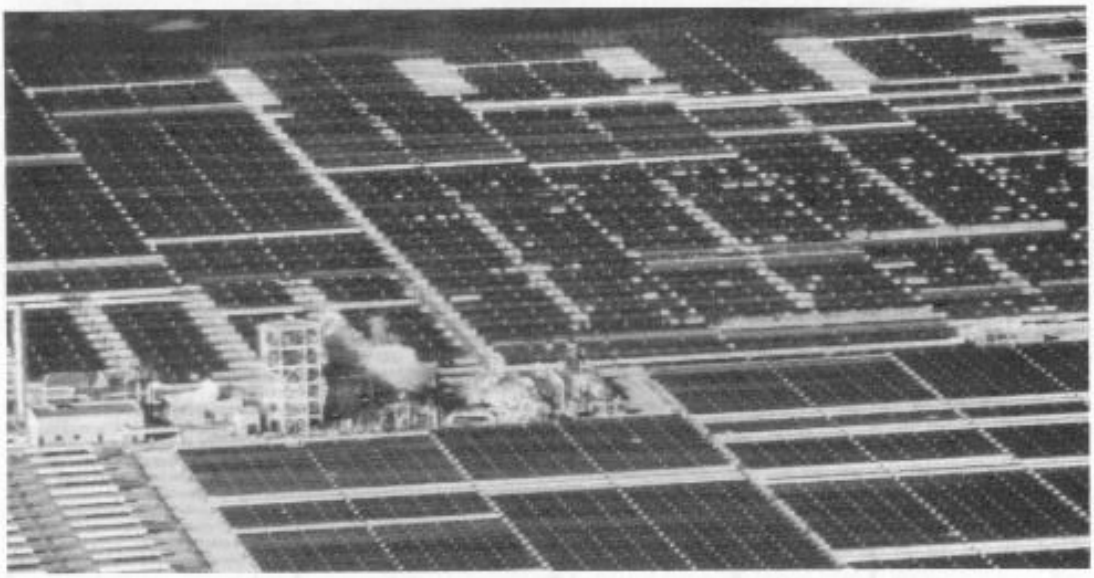

FIGURE 11.31 Solar electric generating station located in the Mohave Desert of California, designed and operated by Luz International Ltd. (Photo courtesy of Southern California Edison.)

Solar Thermal Electric Generating Stations

Large thermal applications of solar energy to produce electrical power are located at two sites in the Mohave desert of California (refs. 65 and 66). These facilities, (Figure 11.31) called *solar electric generating stations–-SEGS*, consist of 14-MW, 30-MW, and 80-MW units employing line-focusing parallel-trough solar collectors to provide heat for reheat steam turbine systems. The SEGS plants in the Mojave Desert make up the world's largest parabolic trough facility. In the year 2000, there were nine plants, which provide a combined capacity of 354 MW (ref. 89). Deployment of additional plants is not expected to occur until at least 2002. When completed, the 12 SEGS units will have a total electrical generating capacity of about 600 megawatts.

Reflected solar radiation from the mirrored-glass sun-tracking horizontal-axis parabolic collectors is focused on an evacuated tubular-heat-collection element through which a heat transfer fluid flows. After leaving the collector, the hot fluid heats water in a steam generator before returning to loop through the collectors, as seen in Figure 11.32. The resulting super heated steam is used in Rankine-cycle reheat steam turbine generators. Cooling towers reject heat from the condensers to the surrounding desert air.

Supplemental heat is provided, when required, by boilers burning natural gas, as shown in Figure 11.32, or, in the newer designs, by gas-fired heaters that heat the collector heat transfer fluid. This supplemental heat is required to ensure that full SEGS plant design output is obtained during the periods of peak demand for electricity in Southern California–from noon to 6 pm between June and September.

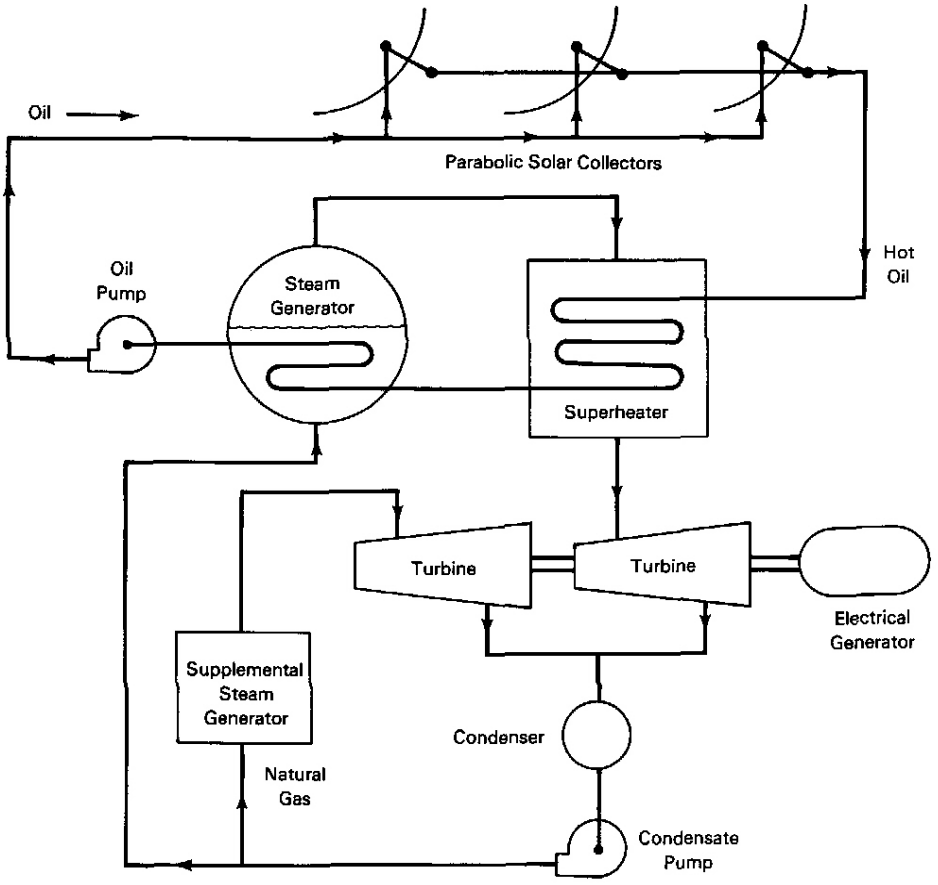

FIGURE 11.32 Schematic diagram of a solar thermal electric generating station.

The large land area required by SEGS plants is evident from Figure 11.31. References 65 and 66 give insight into some of the technical issues faced in the development of SEGS systems; issues that include periodic mirror washing, breakage of the heat collection elements, wind loading, and other operational considerations. Updated information on the SEGS system and other solar-thermal programs is given in references 89 to 92.

Solar Photovoltaics

Photovoltaic cells have gained wide use in recent years as small scale power sources for watches, calculators and other such devices. Less evident to the public is the widespread research and development effort on electric power production using solar photovoltaics. Over two billion dollars in corporate funds have been invested in photovoltaics (ref. 58). The major goal is to provide cheap and efficient direct conversion of solar photons into electricity, using light-sensitive devices with few or

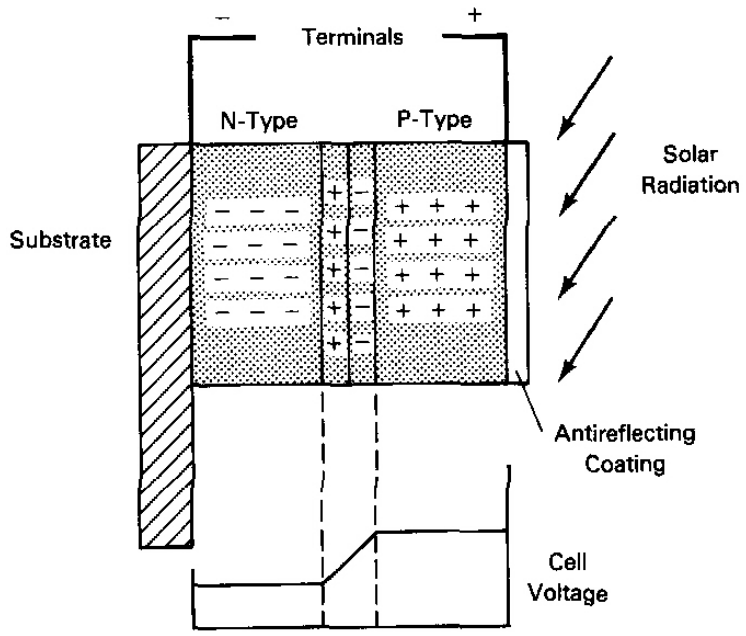

FIGURE 11.33 Crystalline silicon p–n-junction solar cell.

no moving parts. Success could provide a sorely-needed long-term energy source that could benefit most of the peoples of the world.

Photovoltaics rely on specially prepared materials called *semiconductors*, which produce useful current flows when illuminated with solar or artificial radiation. They are typically thin layers of materials such as crystalline silicon, with electrical leads mounted on opposite faces, as shown in Figure 11.33. The silicon is usually mounted on a substrate that provides both structural support and cooling to conduct away heat created by nonproductive radiation absorption. The exposed silicon is usually covered with a transparent, antireflecting protective coating to reduce energy loss via surface reflection.

Crystalline semiconductors are near perfect geometric lattices of atoms that were usually produced by a crystal growth method known as the Czochralski process (CZ), which involves slowly turning a seed crystal of pure silicon as it is withdrawn from a bath of high-purity molten silicon. The CZ process forms an ingot that may be 15 cm in diameter and over one meter long. Thin wafers of silicon are then sliced from the ingot in a slow, delicate process. Other methods, such as casting of square ingots, are in use also. The research and development of more cost-efficient techniques for the large-scale production of semiconductors has a continuing high priority. The extensive use of semiconductors in the computer and electronics industries provides substantial motivation for continued research in semiconductor production methods.

After slicing, silicon crystals are "doped" with occasional special impurity atoms, perhaps a few foreign atoms per million silicon atoms in the lattice. This is typically achieved by heating the wafers and exposing their surfaces to vapors of the doping material, called a *dopant*. This process allows the dopant to diffuse to a controlled depth in the crystals. Semiconducting crystals are electrical insulators at low temperature and weak conductors of electricity at room temperature. The presence of impurities provides charge carriers that substantially enhance the material electrical conductivity when it is exposed to radiation. The following considers how photon absorption in the crystals produces an electrical potential and direct current.

Electrons in semiconductors may exist in a band of bound energy states called a *valence band*. This is analogous to the bound energy levels of individual atoms. As with individual atoms, the absorption of a photon in a semiconductor may change the energy state of an electron. If the photon energy equals or exceeds a threshold level, the electron may be excited into a *conduction band,* where it is free to move throughout the material, obviously enhancing the electrical conductivity of the material.

Consider silicon again as an example of semiconductor behavior. Silicon atoms have four electrons in their outer shell. If impurity atoms in a silicon crystalline lattice have five electrons in their outer shell (atoms such as arsenic or phosphorus) the silicon crystal has an overabundance of electrons (and positive charge) and is therefore known as an *n-type* (negative) semiconductor. The extra electrons associated with impurity atoms are loosely bound just below the conduction band. Small amounts of energy from the thermal motions in the lattice or from absorption of photons allow these electrons from the impurity atoms (called *donor atoms*) to move freely in the crystal. The result is a neutral material containing mobile negative-charge carriers.

Now consider another type of crystalline silicon semiconductor, the *p-type*, which has positive charge carriers. If, in the silicon crystal,, the impurity atoms have three electrons instead of five in their outer shells (as in boron or gallium), the impurity atoms can easily snatch electrons from nearby silicon atoms leaving positively charged silicon sites called *holes* and fixed negative dopant atoms. These impurity sites are called *acceptors* because they draw electrons from silicon atoms, thus creating *positive holes* in the lattice. This type of semiconductor is called a p-type, because the holes are positive charge carriers. When an electron abandons one silicon site for another, a hole disappears at its destination and new hole is created at its point of origin. Thus a p-type semiconductor has holes that may move through the material as positive-charge carriers.

When an external electric field is applied to an n-type semiconductor, electrons will move toward the region of high potential. However, the electrons are restrained by the positive fixed donor sites, resulting in a charge distribution in balance with the applied field. In a p-type semiconductor, its positive holes would move toward low potential until a stable charge distribution with the negative acceptor sites is established. Thus, because of the fixed charges at donor and acceptor sites, the

charge carriers will move just far enough to set up charge distributions that are in balance with the external field.

Consider layers of p-type and n-type semiconductors brought together to form an electrically neutral slab with a common interface called a *p-n junction*. Because of concentration gradients of free electrons and holes across the junction, some electrons from the n-type will cross into the p-type, while holes move a short distance into the n-type. The diffusion of holes and electrons rapidly creates and is balanced by an electric field in a thin space-charge region less than a micron thick, as indicated in Figure 11.33. As a result, the p-type material is at a higher potential than the n-type. Thus the two materials on either side of the junction are each at different potentials without the benefit of an external electric field, thanks to the electric field at the p-n junction.

Now let's consider radiation incident on the p-n semiconductor. Photons have an energy $h\nu$, where h is Planck's constant and ν is the frequency of the radiation. When a p-type material near a p-n junction is irradiated by an energetic photon, the photon may be absorbed, raising an electron into the conduction band and leaving a hole behind. Thus a single photon creates an electron-hole pair. Conduction band electrons readily move across the junction into the n-type material to a region of lower potential energy, while the holes tend to move in the opposite direction and thus remain in the p-material. Likewise, electron-hole pairs created by irradiation of n-type material cause holes to move into the p-material, leaving the electrons behind. Thus the photons provide the energy for a pumping process that separates and selectively drives charges across the interface. These actions increase the positive charge in the p-type and the negative charge in the n-type materials, opposing the electric field produced by diffusion due to charge concentration gradients. This process continues until the electric fields balance each other.

When an external load is connected to the irradiated cell, electrons flow from the n-type material through the external circuit while holes move in the opposite direction. The net current flow through the load is the sum of both the electron flow and the hole flow through the semiconductor layers. Since the number of charge carriers driven through the load depends on the number of photon excitations, the total cell current and power output depend on the junction surface area and on the intensity of solar irradiance.

A silicon solar cell may be 10 cm by 10 cm, and have an open circuit voltage of about 0.5 V. At 10% efficiency it would deliver a power output of 1 W when receiving peak solar irradiance on Earth of 1.0 kW/m^2.

$$\text{Power} = (1.0)(10/100)^2(0.1)(1000) = 1.0 \text{ W}$$

The band gap, or energy separation, between conduction and valence bands is 1.1 eV for silicon p-n junctions. This is the energy necessary to move an electron into the conduction band of the semiconductor.

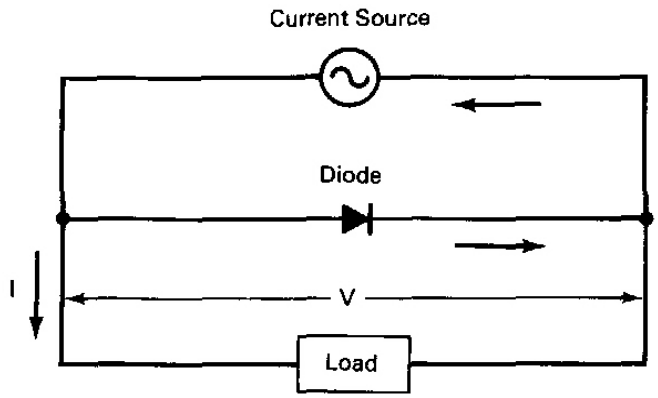

FIGURE 11.34 Solar cell model equivalent circuit.

Thus, to excite electrons into the conduction band, photons must have a frequency equal to or greater than E/h, the photon energy (equal to band gap energy) divided by Planck's constant

$$\nu = (1.1 \text{ eV})(1.602\times10^{-19} \text{ J/eV})/(6.626\times10^{-34} \text{ J-s}) = 2.66\times10^{14} \text{ s}^{-1}$$

and a wave length no greater than c/ν, the speed of light divided by the photon frequency:

$$\lambda = (2.9979\times10^{8} \text{ m/s})(10^{6} \ \mu\text{/m})/(2.66\times10^{14} \text{ s}^{-1}) = 1.127 \ \mu$$

Photons with lower frequencies and longer wave lengths, and therefore energies less than the band-gap energy, cannot raise electrons to the conduction band and may be transmitted through the material without effect. On the other hand, one photon can excite only one electron into the conduction band, and any excess photon energy beyond the band gap value only heats the semiconductor. Thus photon wave lengths greater and less than the bandgap value result in inefficiency in converting incident radiation to electricity.

The p-n junction acts like a combination of a current source and a diode in parallel as shown in Figure 11.34. For a given level of cell irradiation, a cell electrical characteristic may be represented by

$$I = I_{sc} - I_o(e^{qV/kT} - 1) \qquad [\text{A}] \qquad (11.48)$$

where k is the Boltzmann constant, q is the electronic charge, and I_o is called the dark current. The short-circuit current I_{sc} (corresponding to a cell potential difference =0) is proportional to the rate of incident irradiance. The dark current I_o is related to the cell open-circuit potential difference V_{oc} by setting $I = 0$ in Equation (11.48). Thus:

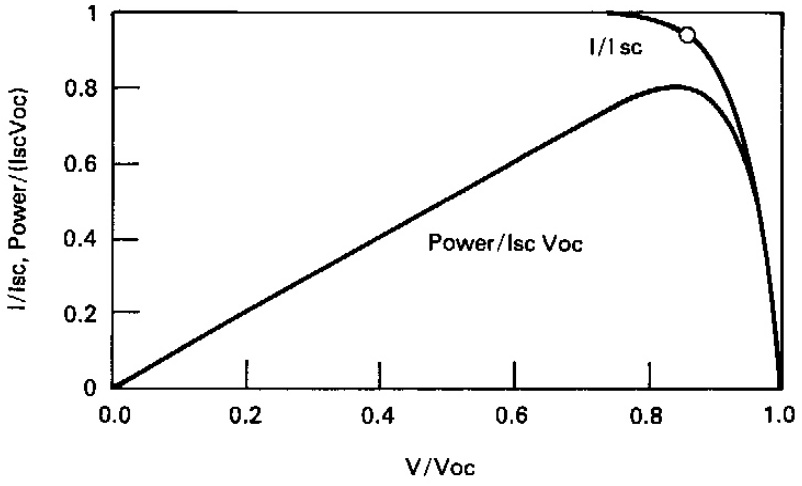

FIGURE 11.35 Ideal photovoltaic cell characteristics.

Thus

$$I_o/I_{sc} = 1/(e^{qVoc/kT} - 1).$$

By combining these two equations, we can write the cell characteristic in nondimensional form as

$$I/I_{sc} = 1 - (I_o/I_{sc})(e^{qV/kT} - 1) = 1 - (e^{qV/kT} - 1)/(e^{qVoc/kT} - 1) \qquad [dl] \qquad (11.49)$$

The cell power output is the product of the current and cell potential difference:

$$P = IV = [I_{sc} - I_o(e^{qV/kT} - 1)]V \qquad [W]$$

Nondimensionalizing the power by dividing it by $I_{sc}V_{oc}$ gives

$$P/I_{sc}V_{oc} = [1 - (e^{qV/kT} - 1)/(e^{qVoc/kT} - 1)](V/V_{oc}) \qquad [dl] \qquad (11.50)$$

The nondimensional current and power characteristics are shown in Figure (11.35). It may be seen from the figure that peak cell power increases linearly with output voltage for small values of voltage, reaches a maximum at between 80% and 90% of the open circuit voltage, and drops rapidly thereafter. The maximum power is about 80% of $I_{sc}V_{oc}$. For given values of I_{sc} and V_{oc}, the maximum power occurs at particular values of current and voltage (indicated by the circle on the current characteristic), and thus at a single load resistance. For other resistive loads the power output is reduced.

EXAMPLE 11.10

For a photocell with an open-circuit voltage of 0.6 V at 350K, evaluate qV_{oc}/kT and the nondimensional current and power at $V/V_{oc} = 0.8$. Propose a simplification of the model given earlier for large values of the voltage parameter.

Solution

For $T = 350$K and $V_{oc} = 0.6$ V, the dimensionless voltage parameter is

$$qV_{oc}/kT = 1.602\times10^{-19}\times0.6 / (1.38\times10^{-23}\times350) = 19.9$$

Using Equation (11.49), the current ratio is then

$$I/I_{sc} = 1 - (e^{0.8\times19.9} - 1)/(e^{19.9} - 1) = 0.9813$$

and the power ratio is

$$P/I_{sc}V_{oc} = (I/I_{sc})(V/V_{oc}) = 0.9813\times0.8 = 0.785$$

It is clear that for large values of the voltage parameter, 1 may be neglected with respect to the exponentials; hence we may write the following excellent approximations:

$$I/I_{sc} = 1 - e^{(qV\text{oc}/kT)(V/V\text{oc} - 1)}$$

and

$$P/I_{sc}V_{oc} = [1 - e^{(qV\text{oc}/kT)(V/V\text{oc} - 1)}](V/V_{oc})$$

The reader may verify numerically the accuracy of these approximations.

The cell efficiency is the ratio of the maximum cell power output to the rate of incident radiant energy normal to the cell, P_m/E_{inc}, where P_m is the product of the cell current and the voltage at maximum power point. For a given irradiance, doubling the cell efficiency implies doubling the cell current and power output. Let us consider a few of the types of energy losses that contribute to low cell efficiency in converting energy from the radiation field into electricity.

It has been seen that in silicon, the minimum photon energy required to create an electron-hole pair is 1.1 ev and that (1) photons with energies less than 1.1 ev are not absorbed by the semiconductor; and (2) the excess energy of photons with greater than the required energy is converted to heat, since a photon can create only one electron-hole pair. For silicon cells, these losses exceed 50% of the incident energy (ref. 11.59). Thus the nature of the solar spectrum and the excitation energy of

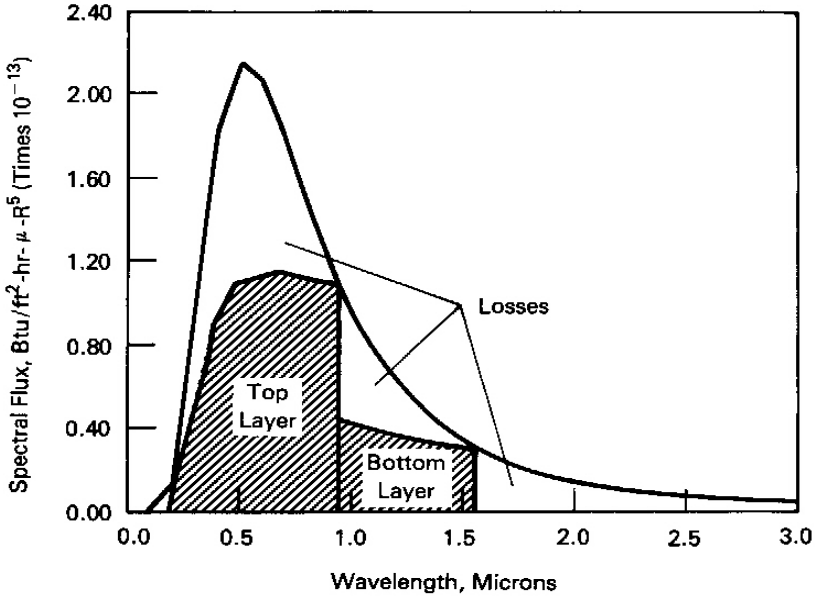

FIGURE 11.36 Spectrum losses in a multilayer two-junction semiconductor.

particular junction materials influences the cells' efficiency. Analyses of these losses indicate that the silicon band-gap energy is lower than optimum for the solar specral distribution. References 39 and 42 indicate that cadmium telluride, CdTe, and gallium arsenide, GaAs, have near-optimum band-gap energies around 1.4 eV for the solar application.

Another loss that contributes to inefficiency is reflection at the cell surface. Antireflection coatings are currently used to reduce this loss to a few percent of the incident energy. When these and other losses are accounted for, a maximum conversion efficiency of single-crystal silicon cells in sunlight is about 25%. Values of 23.2% and 22.3% have been obtained in two laboratories when high efficiency was the objective (ref. 69). The best efficiency of commercial silicon cells is about 15%.

Solar Cell Design

Other semiconducting materials that have received less attention than silicon have been found to use the solar spectrum more efficiently, as indicated above, and thus offer potential for higher conversion efficiency. Research is also in progress on cells made of thin layers of several junction materials that each work best in different parts of the spectrum. Thus, if a top layer converts high-frequency photons efficiently and allows lower frequency photons to pass to a lower layer to be converted by a semiconductor with a lower band-gap energy, a larger part of the spectrum may be used efficiently. For instance, as Figure 11.36 shows for a two junction cell,

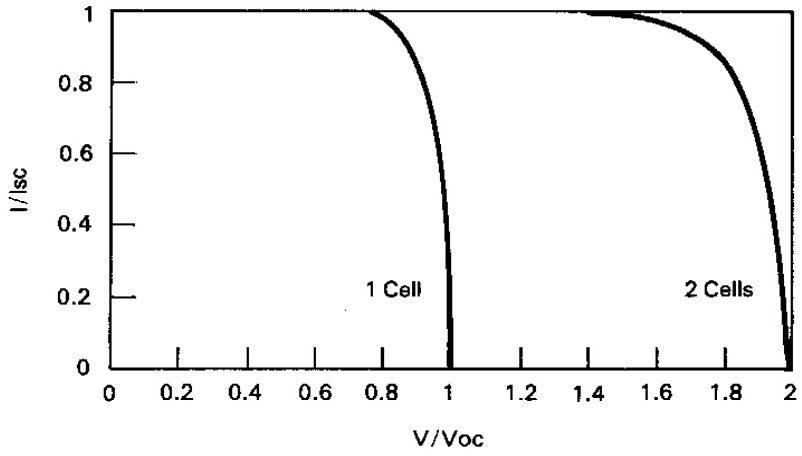

FIGURE 11.37 Photovoltaic cells in series.

ultraviolet and visible wavelength photons may be absorbed near the top junction and infrared photons near the bottom.

Regardless of the individual cell characteristics, in order to achieve power outputs of significance for utility and industrial applications it is necessary to string the cells together in arrays. Identical cells connected in series all have the same current; and their combined voltage is the sum of the individual cell voltages at the given current flow, as shown in Figure 11.37. For example, using a typical value for the open-circuit voltage and the voltage condition for maximum cell power, in order to get a voltage of about 14 V to charge a 12-V battery it is necessary to bring together about

$$14\ V/[(0.5V_{oc}/\text{cell})\ (.8V/V_{oc})] = 35\ \text{cells}$$

in series. For 10-cm by 10-cm cells, such a string would have a maximum power output of about

$$(35\ \text{cells})(1\ \text{watt}/\text{cell}) = 35\ W$$

and an area of $35\times10\times10 = 3500\ cm^2$ or $0.35\ m^2$.

In order to achieve high current flow, it is necessary to connect cells or strings of cells in parallel. In this case the currents are additive for a given cell potential, as seen in Figure 11.38. While high voltages are desirable to reduce ohmic losses and reduce wire size, according to reference 38 limitations on insulations and safety concerns will limit the voltage levels achieved by solar arrays. Since the National Electric Code does not provide for equipment ratings above 250 V DC, higher voltages may imply increased costs for solar power systems.

In the event of cell damage, loss of one cell in a parallel string of cells means the loss of only the power of that cell, whereas loss of a single cell in a series string

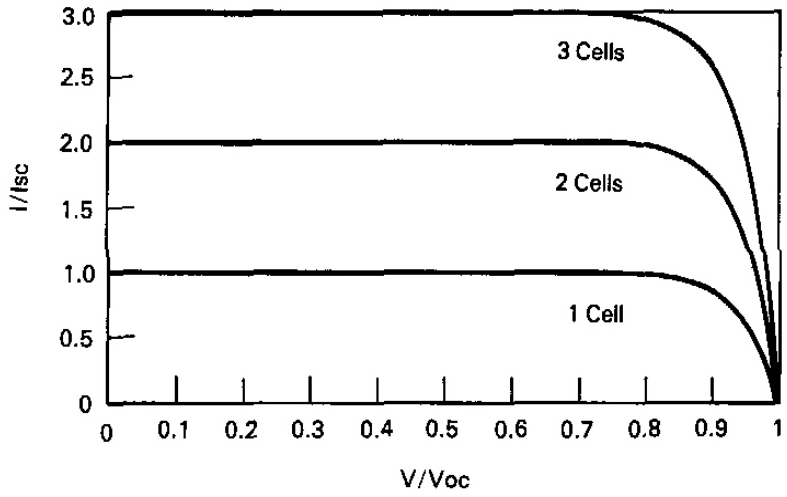

FIGURE 11.38 Photovoltaic cells in parallel.

causes a large loss in power because of the large increase in series resistance of the string. Shading from the sun of a single cell in series has a similar effect, because the reduction in incident radiation cuts the current carrying capability of the cell and hence the entire string. Circuitry is usually provided to allow current to bypass a defective cell.

EXAMPLE 11.11

A near-Earth satellite requires a maximum of 10 kW of electrical power. Estimate the required collector area and the number of 10-cm by 10-cm cells, each having a conversion efficiency of 14%.

Solution

Using a solar constant of 1.357 kW/m^2, the required area is determined by dividing the design power requirement by the amount of the incident radiation that is converted to electricity by the cells:

$$10/[(0.14)(1.357)] = 52.64 \text{ m}^2$$

The number of 10 by 10 cells is then

$$52.64/(10/100)^2 = 5264 \text{ cells}$$

The direct conversion of solar radiation to electricity is very attractive from the point of view of the long-term reliability of the source and environmental

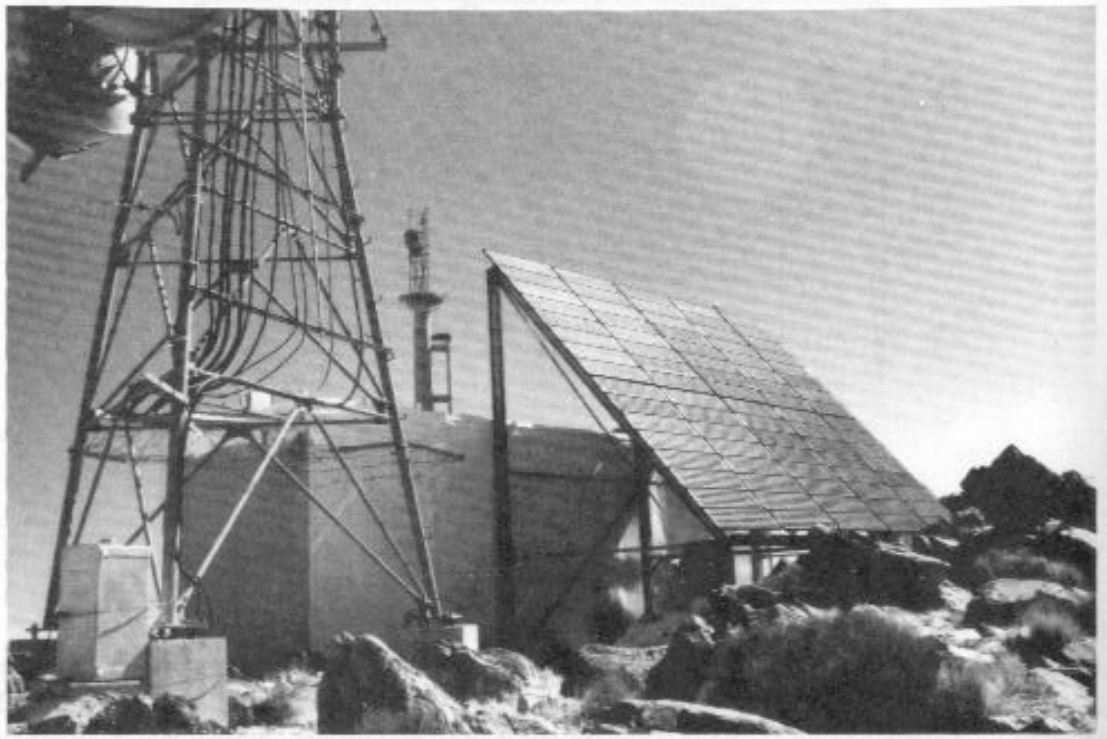

FIGURE 11.39 Remote photovoltaic-powered telecommunications system atop a 2500-ft mountain. (Courtesy of Southern California Edison.)

acceptability. There are, however, several fairly obvious adverse characteristics of solar conversion. First, terrestrial applications suffer from the limited daily availability of sunshine. The frequent coincidence of the daily peak irradiance and utility demand peaks is advantageous but does not compensate for the wide daily variability of the solar source. The occurrence of cloudy days, sometimes several successive ones, and the inevitable daily sunset indicate the need for energy storage if solar energy is to provide a reliable primary source of electricity. For remote, stand-alone locations this implies the use of batteries or other storage devices to satisfy 24 hr/day demand. Figure 11.39 shows a remote photovoltaic-powered telecommunication site located on a mountain top. The system comprises the cell array, the storage batteries, the telecommunications load, and the electronics needed to control battery charging and load matching. The system shown is said to have recovered its cost in a year and to produce annual savings of $60,000.

In industrialized countries, such as the United States, where utility grids penetrate to most parts of the country, linkages with utilities seem to offer the best hope for widespread photovoltaic use, because the existing utility grids can provide the needed backup. Both decentralized and central-station solar conversion appear to be possibilities for utility involvement. Moreover, the Public Utilities Regulatory Policy Act (PURPA) offers other possibilities by encouraging third-party as well as utility and customer ownership arrangements.

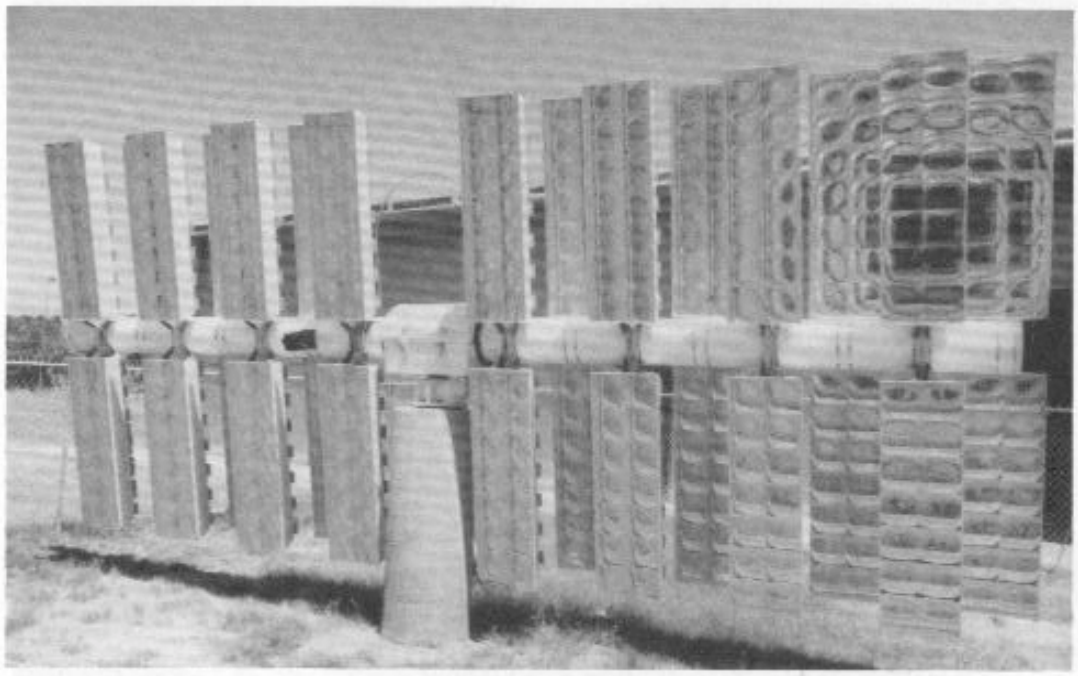

FIGURE 11.40 Sun-tracking, concentrating solar cell system. Fresnel lenses concentrate sunlight by a factor of 100 in each of the fourteen cells in each parquet. The 21-ft long structure produces 2.4 kW of electrical power. (Courtesy of Southern California Edison.)

The high cost and low efficiency of solar cells are major deterrents to their widespread application for power generation. Although the costs of solar cells have been declining and cell efficiencies increasing over the years, solar cells still are economically suited for only a limited number of applications such as those where cost is not a major factor (e.g., military and aerospace applications) or where the alternatives are expensive (e.g., energy sources for remote installations). Nevertheless the annual production of photovoltaics has been increasing and the resulting production experience will help develop production techniques that, together with increased volume, should further drive down their prices. It is likely that the demand for photovoltaic power generation would increase dramatically if solar cells become available in a price range below $1/W, depending on the price of natural gas, oil and coal.

Concentrating Solar Cell Systems

One approach to reducing the cost and increasing the efficiency of photovoltaics is the development of a concentrating solar cell system that focuses radiation on the cell. The use of a Fresnel lens or other type of concentrator increases the incident energy on a given cell area and, consequently, the cell power output. A photograph of such a concentrating array is shown in Figure 11.40. Each of the 14 elements in each

parquet concentrates energy from a 5-inch-square Fresnel lens onto a 1/4-inch silicon cell. Unlike nonconcentrating cells, the concentrating units only function under clear sky conditions and derive no benefit from diffuse radiation.

Cells with high concentration ratios must be cooled because of high solar intensities on the cells. Some of the details of the EPRI-Stanford cell system adapted from reference 63 are given in Figure 11.41. According to that reference and reference 49, efficiencies as high as 28% have been reached in experimental crystalline silicon concentrator cells. Reference 59 suggests that the required high efficiencies for commercialization of concentrating cells are being achieved today and that attention can be focussed on production and cost reduction efforts for this type.

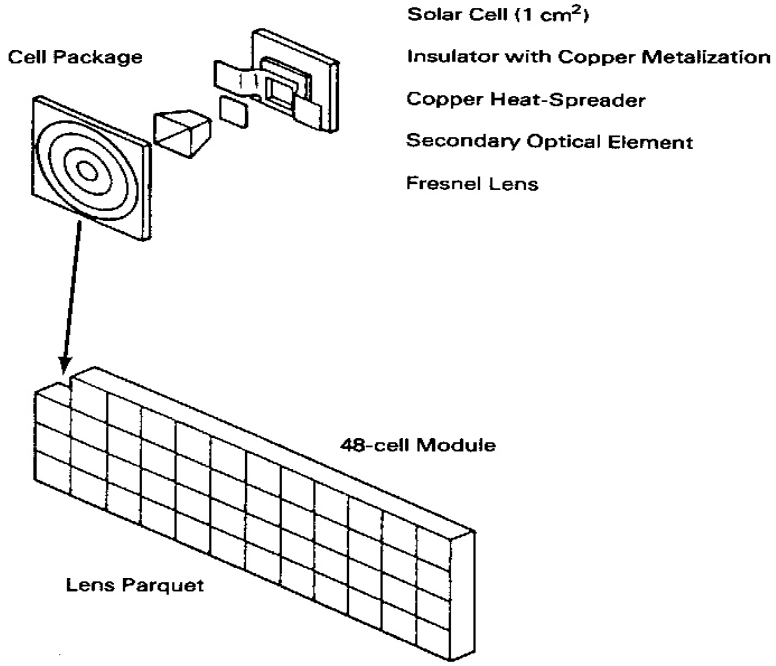

FIGURE 11.41 Some details of a solar concentrator array design.

Designs are being developed for integrating the EPRI-Stanford University concentrator solar cell into full-scale photovoltaic arrays for testing and demonstration.

After manufacture by semiconductor device fabrication processes, each point-contact cell is soldered to a ceramic insulator that is direct-bonded to copper contacts. Atop each cell is bonded a reflecting aluminized secondary optical element that helps a Fresnel lens above it to maintain 500-sun concentration on the cell surface. Mounted in the bottom of a deep-drawn module housing, each cell is in turn mounted on a copper heat-spreader bonded to the inside of the module.

The 48-cell module, an aluminized steel pan measuring 29 × 87 in (750 × 2210 mm) and covered by a parquet of Fresnel lenses, becomes the building block for large arrays comprising 60 modules and having a peak electrical rating of about 18 kW.

The concentrator array, nominally 100 m^2 (about 1000 ft^2), is mounted on a 14-ft (4-m) pedestal that provides structural support and keeps it optimally pointed toward the sun with a computer-controlled, electronic drive-tracking system.

A 100-MW central station generating facility would consist of about 5600 such 18-kW arrays, which, when properly spaced, could occupy over 600 acres (240 ha). The facility could be constructed in 10-MW increments as additional generating capacity is needed.

Adapted from *EPRI Journal* (ref. 63).

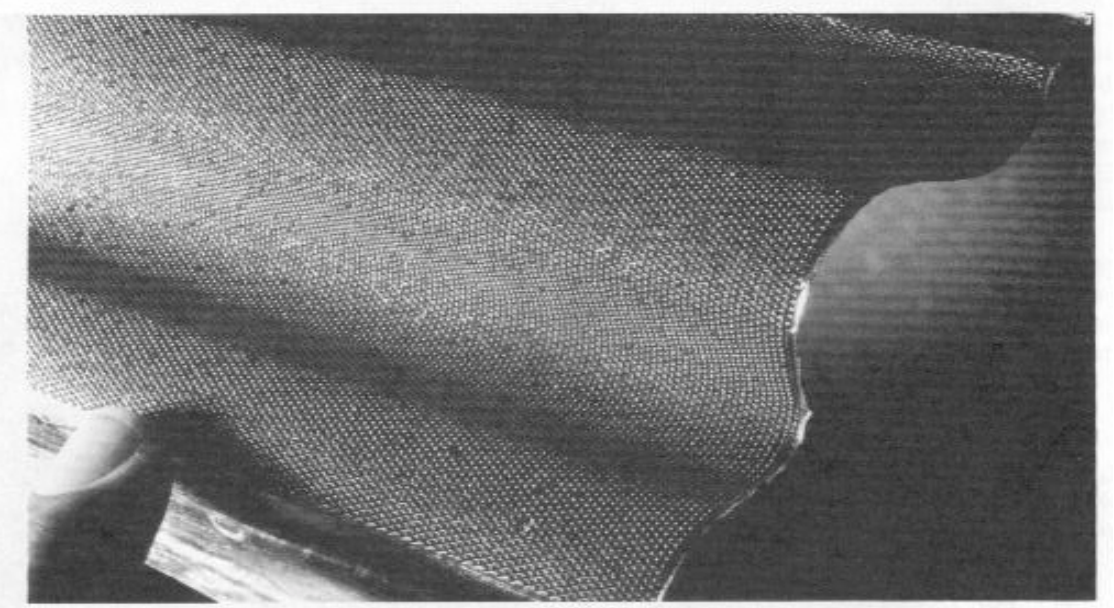

FIGURE 11.42 Advanced photovoltaic (Spheral Solar™) technology offers hope of low-cost, environmentally clean energy. (Photo by Greg O'Loughlin. Courtesy of Southern California Edison.)

Other Approaches

Major reasons for the high cost of solar arrays is the complexity and labor intensiveness of production of high-quality crystalline silicon. Noncrystalline silicon, or *amorphous silicon*, may also be used for photovoltaic cells, but with a practical conversion efficiency limit of about 14%. The best commercially available amorphous cells have an efficiency of about 6%. Crystalline silicon currently has most of the market but amorphous silicon and other non-crystalline semiconductors are receiving considerable research attention. Whereas crystalline cells are cut from carefully grown crystals, amorphous cells may be created by vacuum deposition of a thin film of silicon on a substrate such as glass. While not without problems, manufacturing techniques for amorphous materials appear to offer greater potential for low-cost mass production than those for crystalline cells. One of the current research problems, however, is that amorphous silicon loses some of its effectiveness rapidly upon exposure to light. This has not stopped its use in some applications but is a serious concern.

An exciting approach to photovoltaic power technology was announced in 1991 by Texas Instruments and Southern California Edison. The concept, referred to as Spheral Solar™* technology, involves the use of 17,000 tiny silicon balls per 100 cm^2 supported on flexible aluminum foil sheets, as seen in Figure 11.42. The spheres are metallurgical grade p-type silicon with surfaces doped with an n-type material so that each sphere is an individual solar cell. The spheres are set in perforations in a foil

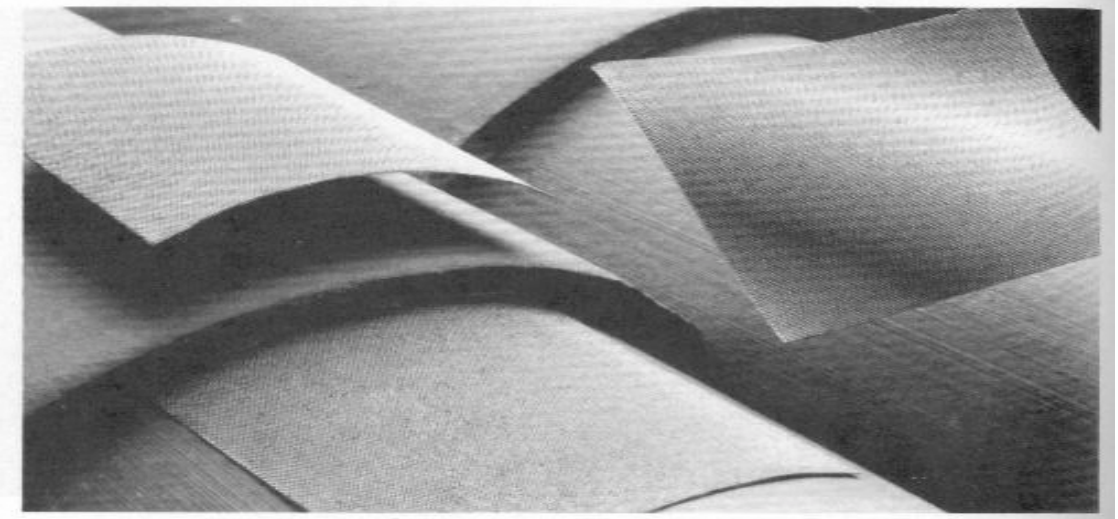

FIGURE 11.43 Spheral solar technology in a potential rooftop application. (Courtesy of Southern California Edison.)

layer that forms the contact with the n-layer. Both sides of the spheres are coated with transparent ethylene vinyl acetate. The rear tips of the spheres are etched, exposing p-type material where another foil layer forms the contact with the p-layer.

Several features claimed for the spheral technology offer hope for a breakthrough in the production of solar electricity:

- The silicon used is inexpensive, low purity, metallurgical grade.
- The technology uses low-cost production methods that provide an almost 100% yield of manufactured laminates.
- Since each sphere is a solar cell, the failure of an individual sphere has a negligible influence on system performance.
- The flexible nature of the laminate makes it adaptable to a wide range of applications (Figure 11.43).

Module efficiencies of about 8–10% are expected (ref. 76). Reference 80 indicates that the highest efficiency attained during R&D testing was 11.5%. A line for pilot production prototype modules was established in 1991, with production commercial planned for 1994. More recent information is available in reference 96.

The application and sales of photovoltaics have been growing continually in the last 20 years. Though photovoltaics continue to offer great hope for large-scale power production, there remains a diversity of opinion regarding the avenues and rates of commercialization of photovoltaics in power production applications (ref. 49).

11.6 A Hydrogen Economy

Coal, natural gas, petroleum, and uranium are all *primary energy sources*, mainly for heat. On the other hand, electricity is a convenient form of energy, or work, derived from a primary source and may therefore may be called a *secondary energy source*. Electricity plays an important role in the world energy system because it is a convenient and inexpensive source of both heat and work. It is used as readily for lighting and cooling as for heating and mechanical power delivery. It is readily transmitted over moderate distances and is relatively safe and non-polluting. Its pervasive influences on society within the world's energy system are such that we have what is sometimes referred to as "an electrical economy."

However, electricity has failed to gain a foothold in most modes of transportation, primarily because of the lack of a compact and flexible means of storing it. Some progress in this area may be anticipated because of renewed interest in electric cars, trucks and other road vehicles. A primary dissatisfaction with electricity as a means of energy application lies in the facts that an electrical economy requires the consumption of about three units of primary energy for each unit of secondary energy produced and that most of the primary energy conversion processes have adverse environmental consequences.

Much interest has been expressed in supplementing or replacing electricity with another secondary energy source, with hydrogen being the leading contender. Methanol, ethanol, liquefied natural gas (LNG), and compressed natural gas (CNG) are other possibilities. A number of advantages may be attributed to employing hydrogen as a secondary energy source:

- Hydrogen may be produced by chemical processes from fossil fuels, by hydrolysis of water with oxygen as a by-product, or by thermal decomposition. According to reference 16, electrolysis cells produce hydrogen at efficiencies between 60 and 69%; 75 to 80% was feasible with 1973 technology, and 85% is expected in a well-developed hydrogen economy.

- Hydrogen can be used as a fuel to produce power with almost no direct environmental pollution, because the principal product is water vapor. Combustion of hydrogen produces no carbon products and therefore no "greenhouse gases." Oxides of nitrogen would remain as pollutants but should be more easily controllable because of the absence of carbon and sulfur-containing pollutants.

- Internal combustion engines can use hydrogen with minor modifications, sometimes with improved efficiency.

- Fuel cells employing hydrogen can be used to produce electricity at high efficiencies not bounded by the Carnot limit and with little environmental impact.

- Hydrogen could be produced by electrolysis at large base-loaded electrical power plants during periods of low demand for electricity, thus providing an opportunity for electrical energy storage when used with fuel cells or other efficient energy converters.

- Hydrogen could be transported in pipelines similar to natural gas pipelines. In some cases, existing pipelines could be used with relatively little modification. Liquid hydrogen has been routinely shipped in special rail cars and trucks for many years.

- Hydrogen can be stored in the same ways that natural gas and helium are stored now, underground or in liquefied form in special storage tanks.

- Hydrogen has a very high heating value on a mass basis but a low volumetric value because of its high specific volume at standard pressure and temperature.

The numerous attractive features of hydrogen as a fuel are to a certain extent offset by some serious concerns, which are the objects of extensive engineering research:

First, the ignition energy of hydrogen is low and the flammability limits are wide, so hydrogen is readily ignited. While this is advantageous in combustion systems, great care must be taken in storing and handling hydrogen. Though an atypical event, the Hindenburg disaster perpetually reminds us of these concerns. On the other hand, because hydrogen is lighter than air and diffuses more rapidly than other gases, it is more readily diluted and disperses quickly, characteristics that tend to reduce fire and explosion hazards.

The hazards associated with using hydrogen gas should not be minimized, but to put things in perspective, we should remember that society has enthusiastically adopted an automobile that commonly carries ten to twenty gallons of gasoline, a very hazardous fuel. Large storage tanks of gasoline are maintained and freely accessed by untrained users in the midst of residential areas. Trucks loaded with gasoline routinely service and pass through these same areas.

Second, hydrogen's high specific volume makes its storage a problem, especially in transportation applications, where space for fuel storage is costly. In addition to storage as a compressed gas, it may be liquefied and stored at cryogenic temperatures, or it may be stored in metal hydrides. In the latter cases, the additional equipment space, expense and complexity must be considered in evaluating feasibility and design.

Finally, while gasoline and natural gas remain readily available and at a modest price, hydrogen will have little opportunity to become established as an important secondary fuel. For ground transportation, as a replacement fuel for gasoline, hydrogen must compete with relatively inexpensive methanol and ethanol (ref. 9). Heavily subsidized ethanol is currently available in the United States in a 10% blend with gasoline and there is considerable interest in compressed natural gas and richer methanol mixtures for ground vehicles (ref. 74)

EXAMPLE 11.12

Using reasonable estimates of unit efficiencies for generation, transport, and utilization, compare the overall energy efficiencies of nuclear-electric and nuclear-hydrogen economies in providing mechanical work.

Solution

For the nuclear-electric economy, mechanical energy is produced in the sequence

Fission →Electricity →Transmission →Electric motor

which, using unit efficiencies in the order given, would have an efficiency of about

$$(0.32)(0.9)(0.9) = 0.259$$

For the nuclear-powered hydrogen economy the appropriate chain is

Fission →Electricity →Electrolysis →Hydrogen →Transmission →Fuel cell →Motor

Here the overall efficiency is estimated to be

$$(0.32)(0.85)(0.9)(0.6)(0.9) = 0.132$$

Note that neither case includes the energy costs of mining and processing nuclear fuel. Nevertheless, this example suggests that, despite hydrogen's many advantages, its use as a secondary fuel may lead to inefficient resource utilization. This conclusion is discussed more fully in reference 16.

One can readily appreciate the beauty of the concept of a solar-energy-driven hydrogen-powered cycle in which hydrogen produced by electrolysis of seawater using solar photovoltaic energy, reacts and delivers power and heat in a high-efficiency and non-polluting fuel cell at the point of use, with product water ascending into the atmosphere, where it eventually returns to the sea as rain. The problems in developing and adopting such a cycle for commercial use are great, but the future needs of Earth are so serious that such concepts at least provide directions in which research should proceed. While the hydrogen economy may not displace the electric economy, when the politics and economics are right, society will find ways to use hydrogen as a supplement to electricity as a secondary fuel.

11.7 Concluding Remarks

It is clear that the seriousness of Earth's energy and environmental problems and the growing diversity of propulsion and power production options ensures stimulating

careers for engineers far into the future. Attractive, mid-term alternatives exist to the conventional, state-of-the-art, coal-burning power plant with advanced scrubber technology. Despite the risks involved, it seems clear that numerous other power options will find commercial use as dictated by local and regional conditions and available technologies and resources.

A recurring question in all of the developments we have discussed exists: Once the feasibility of a new technology has been established, how can it be rapidly brought to a commercial stage in the absence of massive government support for development and demonstration plants? Under existing economic and regulatory structures in the United States, power utilities cannot make massive investments in technologies that involve significant risks or costs that are not competitive with existing methods. The prices and risks of new technologies will remain high, however, until a significant number of units have been ordered that can absorb research, development, and production costs. In many cases it is unlikely that timely U.S. investment capital will be available for demonstration plants to provide visible confidence-building utility experience. While U.S. governmental support exists, it appears that much of the costs and risks, together with the successes, will be borne internationally.

An important long-term question remains: How can humankind make the transition from a resource-depleting, highly polluting society to some semblance of a steady-state, environmentally acceptable, energy economy based on renewable energy sources? This is not a question for the energy conversion engineer alone. Indeed, it involves political, moral, and social issues that transcend the boundaries of science and engineering. Can a smooth transition be achieved that avoids cataclysmic change and minimizes painful societal dislocations? Perhaps the internationalization of the leadership in technology will help bring suitable global responses to these formidable challenges. Regardless of the future course, it must be a responsibility of engineers to keep the long-term needs of Earth and its inhabitants in mind as they make technical decisions to satisfy present needs and desires and continue the quest for technical progress.

Bibliography and References

1. Angrist, Stanley W., *Direct Energy Conversion*, 3rd ed. Newton, Mass.: Allyn and Bacon, 1976.

2. Spitzer, Lyman, *Physics of Fully Ionized Gases.* New York: Wiley-Interscience, 1956.

3. Appleby, A. J., "Advanced Fuel Cells and Their Future Market," *Ann. Rev. Energy*, 13 (1988): 267–316.

4. McLarnon, Frank R., and Cairns, Elton J., "Energy Storage," *Ann. Rev. Energy*, 14 (1989): 241–271.

5. Mellde, Rolf W., "Advanced Automobile Engines For Fuel Economy, Low Emissions, and Multifuel Capability," *Ann. Rev. Energy*, 14 (1989): 425–444.

6. Jackson, John David, *Classical Electrodynamics*. New York: Wiley, 1962.

7. Fraas, Arthur P., *Engineering Evaluation of Energy Systems.* New York: McGraw-Hill, 1982.

8. Vincent, Colin A., et al., *Modern Batteries*. Baltimore: Edward Arnold, 1984.

9. Sperling, Daniel, and DeLuchi, Mark A., "Transportation Energy Futures," *Ann. Rev. Energy*, 14 (1989): 375–424.

10. Fickett, A. P., "Fuel Cell Power Plants," *Scientific American*, December 1978: 70.

11. Society of Automotive Engineers, *Automotive Handbook*, 4th ed., Robert Bosch GmbH, 1996.

12. Mayfield, Manville J., Beyma, Edmund F., and Nelkin, Gary A., "Update on U.S. Department of Energy's Phosphoric Acid Fuel Cell Program." Proceedings of the Sixteenth Energy Technology Conference, February 28–March 2, 1989, Government Institutes, Inc., pp. 184–196.

13. Myles, K. M., and Krumpelt, M., "Status of Molten Carbonate Fuel Cell Technology." Proceedings of the Sixteenth Energy Technology Conference, February 28–March 2, 1989, Government Institutes, Inc., pp. 197-204.

14. Bates, J. Lambert, "Solid Oxide Fuel Cells: A Materials Challenge." Proceedings of the Sixteenth Energy Technology Conference, February 28–March 2, 1989, Government Institutes, Inc., pp. 205–219.

15. Gillis, Edward, "Fuel Cells," *EPRI Journal*, September 1989: 34–36.

16. Harder, Edwin L., *Fundamentals of Energy Production*. New York: Wiley, 1982.

17. Sissine, F., "Fuel Cells for Electric Power Production: Future Potential, Federal Role and Policy Options," in *Fuel Cells:Trends In Research and Applications*, ed. A. J. Appleby. Washington: Hemisphere, 1987.

18. Appleby, A. J., "Phosphoric Acid Fuel Cells," in *Fuel Cells:Trends In Research and Applications*, ed. A. J. Appleby. Washington: Hemisphere, 1987.

19. Appleby, A. J. (Ed.), *Fuel Cells:Trends In Research and Applications*, Washington: Hemisphere. 1987.

20. Ketelaar, J. A. A., "Molten Carbonate Fuel Cells," *Fuel Cells:Trends In Research and Applications*, Ed. A. J. Appleby. Washington: Hemisphere, 1987.

21. Kinoshita, K., McLarnon, R. R., and Cairns, E.J., *Fuel Cells: A Handbook*. U.S. Department of Energy METC-88/6096, 1988.

22. Berry, D.A. and Mayfield, M.J., *Fuel Cells, Technology Status Report*, U.S. Department of Energy METC-89/0266, 1988.

23. Anon., *Fuel Cell Systems Program Plan*, *FY 1990*, U.S.Department of Energy, FE-0106P, October 1989.

24. Huber, W. J., *Proceedings of the First Annual Fuel Cells Contractors Review Meeting*, U.S.Department of Energy METC-89/6105, May 1989.

25. Anon., *1988 Fuel Cell Seminar*. Washington, D.C.: Courtesy Associates, 1988.

26. Feynman, Richard P., Leighton, Robert B., and Sands, Matthew, *The Feynman Lectures on Physics*, Vol. 2. Reading, Mass.: Addison-Wesley, 1964.

27. Anon., *Battery Service Manual*. Chicago: Battery Council International, 1987.

28. Kotz, John C., and Purcell, Keith F., *Chemistry and Chemical Reactivity*. Philadelphia: Saunders, 1987.

29. Goodman, Frank, "Power Electronics for Renewables," *EPRI Journal*, January/February 1988: 44–47.

30. Schaefer, John, "Photovoltaic Operating Experience," *EPRI Journal*, March 1988: 40–42.

31. Peterson, Terry, "Amorphous Silicon Thin Film Solar Cells," *EPRI Journal*, June 1988: 41–44.

32. Dostalek, Frank, "High Concentration Photovoltaics," *EPRI Journal*, March 1989: 46–49.

33. Morris, Douglas, "The Chino Battery Facility," *EPRI Journal*, March 1988: 46–50.

34. Purcell, Gary, and Driggans, Rick, "Electric Vehicle Testing at TVA," *EPRI Journal*, March 1988: 44–46.

35. Anon., *The Storage Battery*. Horsham, Pa.: Exide Corp., 1980.

36. Makanski, Jason, "Fuel Cells Extend Boundaries of Process/Power Integration," *Power*, May 1990: 82–86.

37. Chapman, Alan J., *Heat Transfer.* New York: Macmillan, 1968.

38. Swanson, Theodore D., "Large-Scale Photovoltaic System Design Considerations," *The Handbook of Photovoltaic Applications*. Atlanta, Ga.: Fairmont Press, 1986, pp. 19–32.

39. Van Overstraeten, R.J., and Mertens, R.P., *Physics, Technology, and Use of Photovoltaics*. Boston: Adam Hilger, 1986.

40. McDaniels, David K., *The Sun: Our Future Energy Source*, 2nd ed. New York: Wiley, 1984.

41. Feynman, Richard P., Leighton, Robert B., and Sands, Matthew, *The Feynman Lectures on Physics*, Vol. 3. Reading, Mass.: Addison-Wesley, 1965.

42. Takahashi, K., and Konagai, M., *Amorphous Silicon Solar Cells.* New York: Wiley, 1986.

43. Duffie, John A., and Beckman, William A., *Solar Engineering of Thermal Processes*. New York: Wiley, 1980.

44. Rosa, Richard J., *Magnetohydrodynamic Energy Conversion*, rev. ed. Washington: Hemisphere, 1987.

45. Gregory, Derek P., "The Hydrogen Economy," *Scientific American*, Vol. 228, No.1. (January 1973) 13–21.

46. Gregory, D. P., and Pangborn, J.B., "Hydrogen Energy," *Ann. Rev. Energy*, 1 (1976): 279–310.

47. Cogineni, M. Rao, Andrus, H.E. Jr., and Jones, T.J., "Advanced Energy Systems." Proceedings of the American Power Conference, Vol. 50, 1988, pp. 282–287.

48. Bajura, R. A., and Halow, J.S., " Looking Beyond the Demonstration Plants: Longer-Term, Coal-Based Technology Options." Proceedings of the American Power Conference, Vol. 50, 1988, pp. 49–56.

49. DeMeo, Edgar, et al., "Thin Films: Expanding the Solar Marketplace," *EPRI Journal*, March 1989: pp. 4–15.

50. Wood, Bernard W., *Applications of Thermodynamics*, 2nd ed. Reading, Mass.: Addison-Wesley, 1982.

51. Womack, G. J., *MHD Power Generation: Engineering Aspects*. London: Chapman and Hall, 1969.

52. Soo, S. L., *Direct Energy Conversion*. Engelwood Cliffs, N.J.: Prentice Hall, 1968.

53. Kettani, M. Ali, *Direct Energy Conversion*. Reading, Mass.: Addison Wesley, 1970.

54. Sutton, George W., *Direct Energy Conversion*. New York: McGraw-Hill, 1966.

55. Pitts, Donald R., and Sissom, Leighton E., *Heat Transfer*, Shaum's Outline Series. New York: McGraw-Hill, 1977.

56. Anon., *The Astronomical Almanac.* Washington, D.C.: U. S. Government Printing Office, 1990.

57. Parsons, Robert A. (Ed.), *The ASHRAE Handbook*, HVAC Systems and Applications Volume. Atlanta, Ga.: American Society of Heating, Refrigerating, and Air Conditioning Engineers, 1987.

58. DeMeo, Edgar, "Getting Down to Business with Thin Films," *EPRI Journal*, March 1989: 4–15.

59. Taylor, Roger W., Cummings, John E., and Swanson, Richard M., "High Efficiency Photovoltaic Device Development: An Example of the R&D Process," Proceedings of the American Power Conference, Vol. 47, 1985, pp. 255–259.

60. Bockris, J. O. M., *Energy: The Solar-Hydrogen Alternative*. New York: Wiley, 1975.

61. Williams, L. O., *Hydrogen Power*. Elmsford, N. Y.: Pergamon Press, 1980.

62. Sze, S. M., *Semiconductor Devices Physics and Technology*. New York: Wiley, 1985.

63. Moore, Taylor, et al., "Opening the Door for Utility Photovoltaics," *EPRI Journal*, January–February 1987: 5–15.

64. Griffiths, David, J., *Introduction to Electrodynamics*, 2nd ed. Engelwood Cliffs, N. J.: Prentice-Hall, 1989.

65. Anon., "Solar Electric Generating Stations (SEGS)," *IEEE Power Engineering Review*, August, 1989: 4–8.

66. Anon., "Promise of Solar Energy Being Fulfilled in California," *Power*, October 1989: s32—s36.

67. Romano, Samuel, "Fuel Cells for Transportation," *Mechanical Engineering*, August 1989: 74–77.

68. Hirschenhofer, J. H., "International Developments in Fuel Cells," *Mechanical Engineering*, August 1989: 78–83.

69. Carlson, D. E., "Photovoltaic Techniques for Commercial Power Generation," *Annual Review of Energy*, Vol. 15, 1990, pp. 85–98.

70. MacDonald, Gordon J., "The Future of Methane as an Energy Resource," *Annual Review of Energy*, Vol. 15, 1990, pp. 53–83.

71. Moore, Taylor, et al., "On-Site Utility Applications for Photovoltaics," *EPRI Journal*, March 1991: 26–37.

72. Moore, Taylor, et al., "Thin Films: Expanding the Solar Marketplace," *EPRI Journal*, March 1989: 4–15.

73. Smock, Robert W., "Second Generation Fuel Cell Technology Moves Toward Demos," *Power Engineering*, June 1990: 10.

74. Sapre, Alex R., "Properties, Performance and Emissions of Medium-Concentration Methanol-Gasoline Blends in a Single-Cylinder, Spark-Ignition Engine," SAE Paper 881679, October 1988.

75. Douglas, John, "Beyond Steam: Breaking Through Performance Limits," *EPRI Journal*, December 1990: 5–11.

76. Graff, Eric, Texas Instruments Co. Personal Communication, May 24, 1991.

77. Chase, M. W. Jr., et al., *JANAF Thermochemical Tables*, 3rd ed., J. Phys. Chem. Ref. Data 14, Supplement No. 1, 1985.

78. Douglas, John, et al., "Fuel Cells for Urban Power," *EPRI Journal*, September 1991: 5–11.

79. Howell, John R., Bannerot, Richard B., and Vliet, Gary C., "Solar-Thermal Energy Systems." New York: McGraw-Hill, 1982.

80. Levine, Jules D., et al., "Basic Properties of the Spheral Solar Cell." 22nd Photovoltaic Specialists Conference, Las Vegas, Nev., 1991.

81. "International Fuel Cells: Clean, Reliable Fuel Cell Energy," www.internationalfuelcells.com/index_fl1.shtml (November 14, 2000).

82. Rulseh, Ted, "Fuel Cells: From Promise to Performance," *Grid*, Spring/Summer 2000: 15.

83. "Santa Clara Demonstration Project," www.ttcorp.com/fccg/scdpnew1.htm (November 14, 2000).

84. "Fuel Cell Energy, Carbonate Fuel Cell Manufacturer," www.ttcorp.com/fccg/erc_abt.htm (November 15, 2000).

85. "Welcome to Fuel Cell Energy, Inc.," www.fuelcellenergy.com/homeframe.html (December 9, 2000).

86. "Library of Fuel Cell Related Publications," http://216.51.18.233/biblio.html (November 14, 2000)

87. Archer, David H. and Wimer, John G., " A Phosphoric Acid Fuel Cell Cogeneration System Retrofit to a Large Office Building," Department of Energy FETC-97/1044, April 1997., www.fetc.doe.gov/netltv/index.html (November 15, 2000).

88. "DaimlerChrysler Offers First Commercial Fuel Cell Buses to Transit Agencies," www.hfcletter.com/letter/may00/feature.html (November 15, 2000).

89. "TroughNet Projects - Projects Deployed," www.eren.doe.gov/troughnet/deployed.html (November 23, 2000).

90. “Solar Fact Sheets: Solar Thermal Electricity, Solar Energy Industries Association,” www.seia.org/sf/sfsolthe.htm (November 23, 2000).

91. “Solar Thermal Electric Power Plant,” www.magnet.consortia.org.il/ConSolar/stepp.html (November 23, 2000).

92. “About FPL Energy,” www.fplenergy.com/aboutfpl/solar-1.htm (November 23, 2000).

93. “US Department of Energy PV Home Page,” www.eren.doe.gov/pv/pvmenu.cgi?site=pv&idx=0&body=video.html (November 24, 2000).

94. “Solar Information Center - Photovoltaic generation systems - Kyocera Solar, Inc.,” www.kyocerasolar.com/info/solarenergy.html (November 23, 2000).

95. “Photovoltaics Program,” http://www.sandia.gov/pv/ (November 24, 2000).

96. “TI Seeks Buyer For Spheral Solar Technology,” www.ti.com/corp/docs/press/company/1995/510no.shtml (November 25, 2000).

EXERCISES

11.1* Derive an expression for the battery power output, in terms of E and R_i/R_o, for the linear model discussed in connection with Example 11.2. Nondimensionalize the power by dividing by E^2/R_o. Use a spreadsheet to tabulate and plot the dimensionless power as a function of R_i/R_o.

11.2* Derive an expression for the linear-battery-model power output nondimensionalized by E^2/R_i in terms of the internal-to-external resistance ratio. Use a spreadsheet to tabulate the dimensionless power function, and plot it. Is there a condition that produces an extreme value of the dimensionless power? If so, use calculus methods to derive the condition.

11.3 An automobile storage battery with and open-circuit voltage of 12.8V is rated at 260 A-hr. The internal resistance of the battery is 0.2 Ω. Estimate the maximum duration of current flow and its value through an external resistance of 1.8 Ω.

*Exercise numbers with an asterisk involve computer usage.

11.4 A battery electrical storage plant is to be designed for 20-MW peak power delivery for a duration of four hours. The plant uses 600 A-hr batteries operating at 400 volts DC. Estimate the minimum number of batteries and the current in each during peak operation.

11.5 A hydrogen-oxygen fuel cell operates with a voltage of 0.7 volts with water-vapor product. Calculate the work per kg-mole of hydrogen, in kJ and in kW-hr, and determine the cell efficiency.

11.6 A neighborhood fuel cell power plant is to be designed for an electrical power output of 2000 kW with liquid-water product. Estimate the flow rates of hydrogen and oxygen during peak power production, assuming that an 80% efficient power conditioner is used to convert DC to AC power and the fuel cell efficiency is 55%. What is the plant heat rate?

11.7 A hydrogen-oxygen fuel cell has liquid water as product when it operates at 0.82 volts. What is the electrical energy output in kJ / kg-mole of hydrogen, and the cell efficiency?

11.8 Prepare a typed three-page, double-spaced memorandum outlining the design of the power train of a hydrogen-oxygen fuel-cell-powered automobile, giving the design criteria, system description, and quantitative preliminary design data on the power and fuel supply system.

11.9 A hydrogen-oxygen fuel cell stack produces 50 kW of DC power at an efficiency of 60%, with water vapor as product. What is the hydrogen mass flow rate, in g/s, and the cell voltage?

11.10 A fuel cell power plant is to be designed for an electrical power output of 200 MW with liquid-water product. Estimate the flow rates of hydrogen and oxygen during peak power production with an 85% efficient power conditioner and fuel cell efficiency of 55%. What is the plant heat rate?

11.11 Determine the fraction of the solar spectrum that lies in the visible wavelengths between 0.4 and 0.7 μ. What is the ratio of the energy in this visible range to that in a range of the same width between 2.0 and 2.3 μ?

11.12 It is desired to have a window in a south-facing wall shaded by a 1-m overhang at noon on June 21 and fully exposed to the sun at noon on December 21. Determine the maximum vertical size of the window for a house at latitude 35° north.

11.13 A skylight in a horizontal roof is 10ft. above the floor of the room below. Determine the distance that the image of the skylight on the floor at noon moves between December 21 and June 21 at latitude 30° north. Sketch and label a plan view of the two positions.

11.14 Derive an equation for the duration of daylight as a function of latitude for December 21 and June 21. Use a spreadsheet to create a table and a plot of the hours of daylight as a function of latitude for December 21 and June 21.

11.15 Perform an analysis analogous to Example 11.12, comparing the energy efficiency of using utility central solar photovoltaic electricity with (1) an electric heat pump for space heating and (2) with solar hydrogen production for space heating using a furnace.

11.16 An MHD generator uses helium seeded with cesium at 2200K to give an electrical conductivity of 10 $(\Omega\text{-m})^{-1}$. The gas travels at 1000 m/s in a magnetic field of 3 Webers/m^2. What MHD generator volume is needed to produce 50MW of output power with a load factor is 0.6?

11.17 The electrical conductivity of C_2H_4 burned in oxygen at 3000K with a small amount of potassium seed is 60 $(\Omega\text{-m})^{-1}$. An MHD generator operates with a gas velocity of 1000 m/s, the magnetic field intensity is 5 tesla, the channel is 1 meter square in cross-section, and the load factor is 0.5. What is the open-circuit voltage, the load potential difference, and the short-circuit and operating current density? If the electrode area is 50% of the wall area and the channel is 10 m long, what is the current and the power output?

11.18 Prepare a preliminary design of a solar photovoltaic system to provide 1.0 kW of stand-alone, 24 hour / day power to a travel trailer. Write a report giving details, including a schematic of the overall system, a cost estimate, the cell array design, and a discussion of the assumptions on which the design is based.

11.19 Estimate the electrical power requirement in kW, of a 1400-ft^2 floor area (three bedroom home) with three occupants. Using your home power estimate, predict the power requirement for a city of 300,000 people. Use these results to estimate the area of silicon solar cells required to satisfy the community power requirements. Write a short narrative discussing your assumptions and analysis.

11.20 Estimate the efficiency of a parquet of an EPRI-Stanford concentrating solar cell.

11.21 According to reference 65, a 400-MW expansion of the SEGS plants in southern California is expected to cost $1.4 billion. What is the expected capital cost of the generation facilities, in dollars per kW of capacity? Estimate the minimum cost of electricity per kW-h generated by the new facilities if they are operated at full capacity for six hours per day for 30 years.

11.22 Evaluate the efficiency of a solar-photovoltaic-powered hydrogen economy for comparison with the nuclear-powered version given in Example 11.12. Consider the cases where the energy source is (a) photovoltaic electricity, and (b) the sun.

11.23 Assuming 8% efficiency for a spheral solar laminate, what is the maximum electrical output of a one square meter sheet? Estimate the peak and the annual electrical loads for three-person family home. Determine the required area for a fixed spheral solar installation. Indicate clearly the assumptions made.

11.24 Assuming 10% efficiency for a spheral solar laminate, what is the maximum electrical output of a one square foot sheet? Estimate the peak and the annual electrical loads for three-person family home. Determine the required area for a fixed spheral solar installation. Indicate clearly the assumptions made.